MASARYKOVA UNIVERZITA
Přírodovědecká fakulta
Ústav teoretické fyziky a astrofyziky

Bakalářská práce

Brno 2023 Michaela Ďuríšková

MASARYKOVA
UNIVERZITA
PŘÍRODOVĚDECKÁ FAKULTA
ÚSTAV TEORETICKÉ FYZIKY A ASTROFYZIKY

Efekt vakuové disperze na GRB

Bakalářská práce

Michaela Ďuríšková

Vedoucí práce: Mgr. Samuel Kováčik, Ph.D. **Brno 2023**

Bibliografický záznam

Autor:	Michaela Ďuríšková Přírodovědecká fakulta, Masarykova univerzita Ústav teoretické fyziky a astrofyziky

Název práce:	Efekt vakuové disperze na GRB
Studijní program:	Fyzika
Studijní obor:	Astrofyzika
Vedoucí práce:	Mgr. Samuel Kováčik, Ph.D.
Akademický rok:	2022/2023
Počet stran:	vii + 41
Klíčová slova:	kvantový prostor; vakuová disperze; hraniční anomálie; Planckova škála; GRBAlpha; GRB 221009A

Bibliographic Entry

Author:	Michaela Ďuríšková Faculty of Science, Masaryk University Department of Theoretical Physics and Astrophysics

Title of Thesis:	Vacuum dispersion effect on GRB
Degree Programme:	Physics
Field of Study:	Astrophysics
Supervisor:	Mgr. Samuel Kováčik, Ph.D.
Academic Year:	2022/2023
Number of Pages:	vii + 41
Keywords:	quantum space; in-vacuo dispersion; threshold anomaly; Planck scale; GRBAlpha; GRB 221009A

Abstrakt

Předkládáme studii věnovanou dvěma potenciálně pozorovatelným efektům teorie kvantové gravitace, což je teorie předpovídající porušení Lorentzovy invariance při dosažení mikroskopické Planckovy škály. Zaměřujeme se na jev hraniční anomálie, kde odvozujeme modifikovaný vztah pro anihilaci fotonů respektující vliv kvantové gravitace. Zkoumáme pozorovatelnost efektu vakuové disperze u dvou nejenergetičtějších gama záblesků, které kdy lidstvo pozorovalo: GRB 221009A a GRB 230307A. Analýza je provedena na datech z družice GRBAlpha. Zjistili jsme, že detektor GRBAlpha není schopen se svým časovým rozlišením rozeznat potenciální vakuovou disperzi. Nakonec diskutujeme možná vysvětlení rostoucího a klesajícího trendu pozorovaných závislostí.

Abstract

We present a study dedicated to two potentially observable effects of a quantum gravity theory, the theory predicting Lorentz invariance violation when reaching a microscopic Planck scale. We focus on the threshold anomaly phenomenon where we derive a modified threshold relation for photon annihilation, respecting the influence of quantum gravity. We investigate the observability of the in-vacuo dispersion effect on the two most energetic gamma-ray bursts ever observed by humankind, GRB 221009A and GRB 230307A. The analysis is performed on data from the CubeSat GRBAlpha. We have found that the GRBAlpha detector is not capable to distinguish potential in-vacuo dispersion with its temporal resolution. Finally, we discuss the possible explanations for the increasing and decreasing trend of the observed dependencies.

MASARYKOVA UNIVERZITA
PŘÍRODOVĚDECKÁ FAKULTA
KOTLÁŘSKÁ 2, 611 37 BRNO
IČ: 00216224
DIČ: CZ00216224

ZADÁNÍ BAKALÁŘSKÉ PRÁCE

Akademický rok: 2022/2023

Ústav:	Ústav teoretické fyziky a astrofyziky
Studentka:	Michaela Ďuríšková
Program:	Fyzika
Specializace:	Astrofyzika

Ředitel *ústavu* PřF MU Vám ve smyslu Studijního a zkušebního řádu MU určuje bakalářskou práci s názvem:

Název práce:	Efekt vakuové disperze na GRB
Název práce anglicky:	Vacuum dispersion effect on GRB
Jazyk závěrečné práce:	angličtina

Oficiální zadání:
There are various hypotheses for the quantum theory of gravity. They differ in many aspects but (mostly) share a common feature—the existence of a quantum structure of space. This structure results in a dispersion law that does not require the presence of any matter and can take place even in a vacuum. This effect is closely related to various models of Lorenz invariance violation. It is expected that is phenomenon becomes dominant at the Planck energy scale and therefore might not be accessible by laboratory experiments. However, the minuscule effect can pile up over large travel times a particle spends traveling through empty space. In this thesis, we will investigate possible observational features of the vacuum dispersion effect on GRB signals, with the recent signal GRB 221009A as a prominent example.

Vedoucí práce:	Mgr. Samuel Kováčik, Ph.D.
Datum zadání práce:	11. 11. 2022
V Brně dne:	22. 5. 2023

Zadání bylo schváleno prostřednictvím IS MU.

Michaela Ďuríšková, 22. 5. 2023
Mgr. Samuel Kováčik, Ph.D., 22. 5. 2023
RNDr. Luboš Poláček, 22. 5. 2023

Poděkování

Na prvom mieste by som sa rada poďakovala môjmu vedúcemu práce Mgr. Samuelovi Kováčikovi, Ph.D. za jeho ochotu, cenné rady a trpezlivosť pri vedení tejto bakalárskej práce. A najmä za čas, ktorý mne a tejto práci venoval. Ďalej by som sa rada poďakovala RNDr. Jakubovi Řípovi, Ph.D. za pomoc a rady pri spracovávaní dát z družice GRBAlpha. Veľká vďaka patrí taktiež mojej rodine a priateľom za podporu počas celého štúdia.

Prohlášení

Prohlašuji, že jsem svoji bakalářskou práci vypracovala samostatně pod vedením vedoucího práce s využitím informačních zdrojů, které jsou v práci citovány.

Brno 22. května 2023 .....

Michaela Ďuríšková

Contents

Introduction

Astrophysics is, as we know it nowadays, a branch of physics seeking to understand a universe as a whole by explaining the behavior of astronomical objects and their mutual interactions through multiple fields such as electromagnetism, mechanics, thermodynamics, or general relativity. The problem comes when we try to incorporate quantum physics into our description of the universe involving the theory of gravity — with today's knowledge, we are unable to explain both disciplines with the same approach. This is when the potential theory of quantum gravity comes into play.

Quantum gravity theory strives to unify the theory of gravity with quantum physics and therefore give us a complete view of the true nature of the universe. Despite its important significance, quantum gravity does not present a main focus in the astrophysical community. One of the reasons is the overall difficulty to observe potential signs that might be able to confirm this theory. Quantum gravity predicts that space-time itself must have a quantum structure on a microscopic Planck scale. This scale is so minuscule that reaching it to observe the potential effects of quantum gravity is almost impossible, even with state-of-the-art particle accelerators. The only astrophysical apparatus with the greatest potential to get close to the Planck scale are cosmological gamma-ray bursts.

The essence of quantum gravity theory lies in the modification of a standard energy-momentum dispersion relation. The modification leads to the potential dependence of the speed of massless particles on their energies. In other words, quantum gravity contradicts Einstein's special relativity postulate about the constant speed of light.

Using the modified dispersion relation, one can derive the possible observable effects of quantum gravity. One of them is the threshold anomaly, a theory that explains the observation of ultra-high energy photons which are according to standard physics forbidden for us to detect because of their annihilation with low-energy background photons. Another effect is the in-vacuo dispersion, a phenomenon claiming that we should observe a time delay in the arrival time of two simultaneously emitted photons of different energies. The more energetic the photon is, the more significant the time delay should be.

In our thesis, we first get familiar with the theory of quantum gravity and the modified dispersion relation. We continue with the threshold anomaly effect where we try to derive a modified threshold relation that considers quantum gravity. Thereafter, we introduce the in-vacuo dispersion effect. We conduct the analysis on real GRBAlpha data where our goal is to observe the potential time delay between simultaneously emitted photons of different energies. We discuss the obtained results and conclude with the contribution to the future of quantum gravity phenomenology.

The quantum theory of gravity

1.1 Introduction to the quantum space

One of the greatest physical problems faced by scientific society is how to create a ”theory of everything”, a theory that will unite quantum physics with the theory of gravity. Despite the problem being studied for more than 90 years (Amelino-Camelia, 2002), nowadays we still have only hypothetical theories waiting to be proved by the experiments. One of the candidates is a well-known string theory, which is based on the idea that fundamental objects are not considered as point particles, but as pieces of string. The different modes of vibration of the string than represent different elementary particles that vibrate in space-time and result in a rich structure (Bedford, 2011). Another candidate can be a loop quantum gravity, which represents a canonical quantization of general relativity (Bodendorfer, 2016). All of these potential candidates have one thing in common — they predict that space-time itself must have a structure on a microscopic scale. By the microscopic scale is meant the Planck scale, derived and discovered by the famous physicist Max Planck. Therefore, reaching this scale means the standard physical model as we know ceases to make sense and the effects of quantum gravity start to dominate.

1.1.1 Planck Scale

In 1900, the German physicist Max Planck presented in his paper a new system of units (Planck, 1900). This system, named after his discoverer a ”Planck system of units” is now considered as a part of diverse systems of natural units. Using only four fundamental constants, Planck was able to derive relations for natural physical scales of mass, time, and length (Bolotin & Yanovsky, 2016). By fundamental constants is meant:

- c, which stands for the speed of light. This constant presents the limit value of speed and signifies the influence of the theory of special relativity.
- $\hbar$, which stands for the reduced Planck constant. This constant also presents the limit value but signifies the influence of quantum mechanics.
- G is the gravitational constant, in this case presenting a value that fixes the absolute value of interaction strength (Bolotin & Yanovsky, 2016).
- k represents the Boltzmann constant. Originally included as a fundamental constant in the Planck paper from 1900, but in the resulting relations for the scales of mass, time and length do not take a role.

Having the four fundamental constants presented, the resulting relations for Planck scales of mass, time, and length are (Bolotin et al., 2020):

$$\begin{aligned} m_{\mathrm{Pl}} &= \sqrt{\frac{\hbar c}{G}} \simeq 2.18 \times 10^{-8}\ \mathrm{kg}, \\ t_{\mathrm{Pl}} &= \sqrt{\frac{\hbar G}{c^3}} \simeq 5.39 \times 10^{-44}\ \mathrm{s}, \\ l_{\mathrm{Pl}} &= \sqrt{\frac{\hbar G}{c^5}} \simeq 1.60 \times 10^{-35}\ \mathrm{m}. \end{aligned} \tag{1.1}$$

Besides the fundamental relations formulated in 1.1, it is possible to determine also derived Planck relations. For our work, studying the theory of quantum gravity, the essential one is the Planck energy, where the Planck energy presents an inversion to Planck length. The equation is given as (Lacki, 2015):

$$E_{\mathrm{Pl}} = \sqrt{\frac{\hbar c^5}{G}} \simeq 1.22 \times 10^{28}\ \mathrm{eV}. \tag{1.2}$$

Revealed Planck scale represents a characteristic scale for the study of the theory of quantum gravity. We are familiar with this approach and the influences of the different scales also in other physical fields. If the velocity of an object gets close to the speed of light, Einstein's general relativity with its effects takes the role. If we study the behavior of an object on microscopic scales, we must consider the effects of quantum mechanics to describe such behavior. Similarly, in the quantum gravity case, we predict that each of the resulting values obtained from relations 1.1 and 1.2 represent an imaginary border from which a standard physical model breaks down because of the violation of Lorentz symmetry. On these scale levels, a new physics takes the role. It is apparent that reaching the energy levels in the order of the equation 1.2 is impossible for laboratory experiments nowadays. The only apparatus close enough to the Planck energy is gamma-ray bursts (GRBs).

1.2 Mathematical-physical approach to quantum gravity

A mathematical expression of our space-time is described by the flat Minkowski space (Minkowski, 1909), a four-dimensional space composed of three spatial and one temporal dimension. An event in Minkowski space (a point in four-dimensional space-time) can be expressed by a contravariant four-vector as follows:

$$x^i = (x^0, x^1, x^2, x^3) = (ct, \vec{x}). \tag{1.3}$$

The existence of Minkowski's space is strongly linked to Einstein's theory of relativity with its postulates. The first postulate explains that all of the physical laws remain the same for all inertial systems, whereas the second postulate speaks about the constant value of the speed of light for all inertial observers. Lorentz symmetry then completes this postulates with the fact that all transformations of physical laws and their equations between observers remain invariant.

Now we move from the macroscopic world with its relativistic theory to the microscopic world affected by quantum physics. As we know from classical quantum mechanics, we can't measure both the position and momentum of a particle with absolute precision. The more we try to determine the value of one quantity, the more we lose information about the second one. This important principle has its own name — The Heisenberg uncertainty principle. The principle originates in the noncommutativity between two operators, for example between the mentioned position and momentum operators:

$$[\hat{x}, \hat{p}] \neq 0, \tag{1.4}$$

where the inequality to zero means that the two operators failed to commute.

Quantum gravity theory predicts non-classical features of space-time and modification of our description of flat Minkowski space-time. The basis of the theory originates in the deformation or even violation of the Lorentz symmetry when approaching the microscopic Planck scale. The idea of quantization of space-time structure leads to discreteness, resulting in the noncommutative property of Minkowski space-time at the Planck scale (Amelino-Camelia, 2002). In the words of quantum mechanics, we are not able to measure precisely the position of a point, subsequently, we say that the space-time coordinates do not commute (Doplicher et al., 1994):

$$[\hat{x}_i, \hat{x}_j] \neq 0. \tag{1.5}$$

1.2.1 Modified dispersion relation

In Galileian relativity, described by classical mechanics with velocities a lot smaller than the speed of light, we are familiar with the energy-momentum dispersion relation in the following form:

$$E = \frac{\vec{p}^2}{2m}, \tag{1.6}$$

where momentum is expressed as $\vec{p} = m\vec{v}$. Einstein's special relativity presented a needed modification of this relation with the increasing velocity to the value of the speed of light. The dispersion relation in the observer-independent relativistic scale acquired the form:

$$E^2 = \vec{p}^2 c^2 + (mc^2)^2. \tag{1.7}$$

Physicists are convinced that we must adopt a similar scenario in the case of quantum gravity. Because of the hypothesis about the deformation of space-time symmetries, the modification of the energy-momentum dispersion relation takes the role as we are reaching the Planck scale. The modified dispersion relation caused by the quantum gravity effects has in general the form (we stress that in the relations considering quantum gravity is c, $\hbar$ and G set to 1) (Amelino-Camelia, 2013):

$$E^2 \simeq \vec{p}^2 + m^2 + \lambda \vec{p}^2 E, \tag{1.8}$$

where the modification is provided by the parameter λ. This parameter should have a dimension of length — we assume that it has to have a value in the orders of Planck length. In our thesis, we will adopt and use the modified dispersion relation presented in the work

of Kováčik & Prešnajder (2013). In their work, they investigated quantum mechanics in 3D noncommutative space using the rotationally invariant commutation relation of coordinates:

$$[x_i, x_j] = 2i\lambda\varepsilon^{ijk}x_k, \tag{1.9}$$

where $i, j, k = 1, 2, 3$ and ε stands for the permutation Levi-Civita symbol. They obtained the modified dispersion relation in the following form:

$$\left(\frac{1}{\lambda} - \lambda\hat{H}_0\right)^2 = \frac{1}{\lambda^2} - \hat{v}_j^2, \tag{1.10}$$

where $\hat{H}_0$ is a free Hamiltonian — a noncommutative analog to the kinetic part of a Hamiltonian and $\hat{v}_j$ is a velocity operator. We will use the rewritten forms of the relation 1.10 as follows:

$$\hat{v}_j^2 = 2\hat{H}_0 - \lambda^2\hat{H}_0^2, \tag{1.11}$$

$$\hat{H}_0 = \frac{1}{\lambda^2}\left(1 - \sqrt{1 - \lambda^2\hat{v}_j^2}\right). \tag{1.12}$$

We stress that, when using the presented modified dispersion relation, we work with the eigenvalues and eigenvectors of the operators with the subsequent neglect of operator notation.

Threshold anomaly

2.1 Standard threshold relation

One of the hypothetical consequences of the quantum gravity theory is the modification of the standard threshold relation, originally derived from a theory of special relativity. The approach of standard physics tells us that ultra-high energy photons cannot propagate along cosmic space without being attenuated. Such phenomena occur because of the annihilation of high-energy photons with the ubiquitous low-energy background photons, where the occurring severe absorption follows the reaction $\gamma + \gamma \rightarrow e^+ + e^-$. By low-energy background photons are usually meant cosmic microwave background photons (CMB) or extragalactic background light photons (EBL) (Li & Ma, 2021).

The condition for the energy of an ultra-high energy photon to annihilate with the background photon to form an electron-positron pair can be derived using the law of energy-momentum conservation (Li & Ma, 2023). The resulting equation is given as:

$$E \geq E_{\text{th}} = \frac{m_e^2}{\varepsilon_b}, \tag{2.13}$$

where E_{th} is the energy of ultra-high energy photon, ε_b is the energy of background photon and m_e is a mass of an electron.

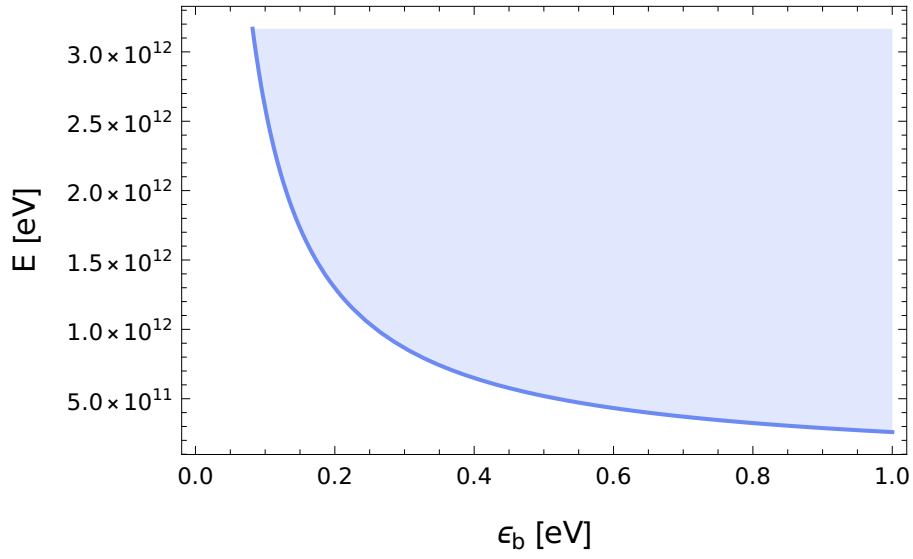

Figure 2.1: Standard threshold illustrated for ultra-high energy photons and the low-energy EBL photons. The annihilation is allowed to occur in the blue-filled part of the graph.

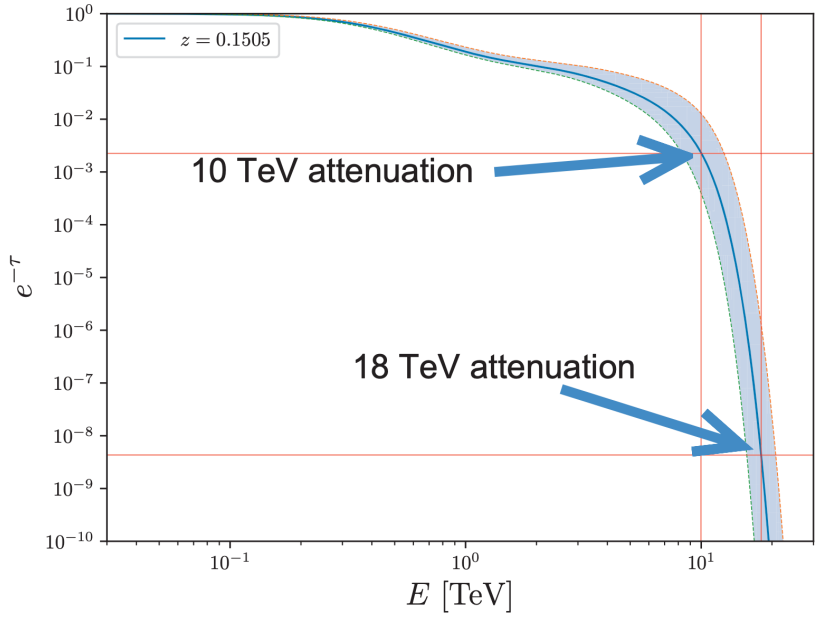

Figure 2.2: The attenuation significance for ultra-high energy photons with the redshift z = 0.1505. The figure was retrieved from the work of Li & Ma (2023), where model and data were taken from Domínguez et al. (2011) and [e3].

The relation 2.13 reveals the existence of a lower threshold above which the annihilation is allowed to occur, and the nonexistence of the upper threshold, meaning we should not be able to observe all photons exceeding the lower threshold. However, the detection of a GRB 221009A with its most energetic photons reaching dozens of TeV (more in subsection 4.2) presents a sign of a possible violation of Lorentz symmetry and a subsequent modification of the known threshold. By applying the dispersion relation presented in 1.12 to the approach of Li & Ma (2021), we will try to derive in the following subsection a modified threshold relation which will include the influence of quantum gravity. We stress that until the end of the chapter, we consider $\varepsilon_b = 1$ eV.

2.2 Derivation of the modified threshold relation

Before all else, relation 1.12 needs to be rewritten as a function of momentum. For that, we use Legendre transformation as follows:

$$\frac{\delta H_0}{\delta v} = \frac{v}{\sqrt{1-\lambda^2 v^2}} =: p. \tag{2.14}$$

Applying $v = \frac{p}{\sqrt{1+\lambda^2 p^2}}$ we obtain:

$$H_0 = \frac{1}{\lambda^2}\left(1 - \sqrt{1-\lambda^2 \frac{p^2}{1+\lambda^2 p^2}}\right). \tag{2.15}$$

To complete the modified vacuum dispersion relation, we assume $H_0 \sim p$ as a relativistic approximation:

$$H_0 = \frac{2}{\lambda}\left(1 - \sqrt{1 - \frac{\lambda p}{1+\lambda p}}\right). \tag{2.16}$$

Following the energy-momentum conservation relation presented in the work of Li & Ma (2021) with our relation 2.16, we are able to write:

$$m_e^2 = \left(\frac{H_0 + \varepsilon_b}{2}\right)^2 - \left(\frac{p - \varepsilon_b}{2}\right)^2, \tag{2.17}$$

and subsequently:

$$4m_e^2 = H_0^2 + 2\varepsilon_b(H_0 + p) - p^2. \tag{2.18}$$

Now we apply Taylor expansion to simplify the terms with Hamiltonian from previously obtained relation, whereas otherwise we would need to solve it numerically:

$$\begin{aligned} H_0^2 &\approx p^2 - \frac{3\lambda p^3}{2} + \mathscr{O}[\lambda^3], \\ H_0 + p &\approx 2p + \mathscr{O}[\lambda^2]. \end{aligned} \tag{2.19}$$

After a few adjustments, the final modified threshold relation acquires the following form:

$$\lambda = \frac{8\varepsilon_b}{3p^2} - \frac{8m_e^2}{3p^3}. \tag{2.20}$$

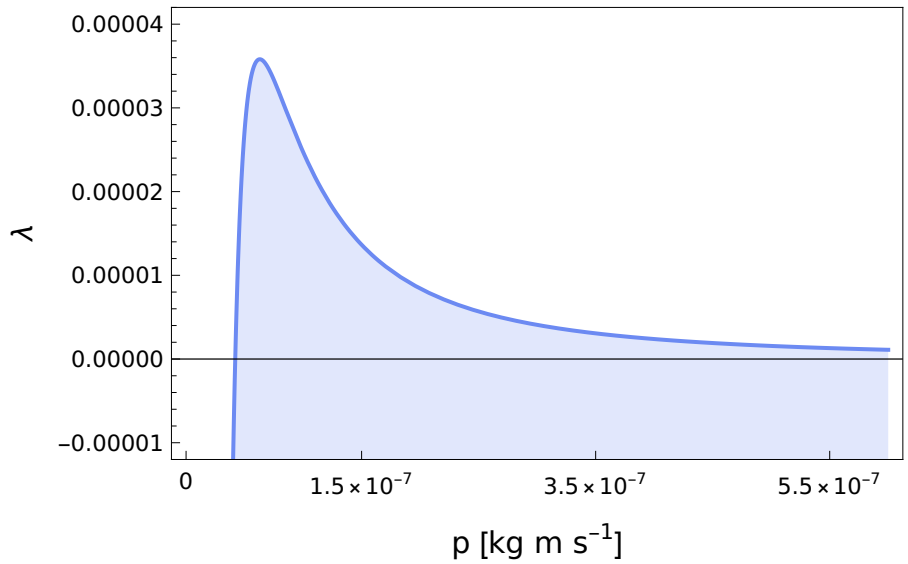

Figure 2.3: Derived modified threshold relation considering Lorentz invariance violation. The blue-filled area below the curve presents a part where annihilation is allowed to occur.

Figure 2.3 reveals different behavior of threshold depending on a value of parameter λ. We consider only $p > 0$, whereas $p < 0$ does not make sense. Also, we highlight two main points of the curve. First, the point intersecting the x-axis ($\lambda = 0$), which correctly signify the standard threshold where $p_0 = \frac{m_e^2}{\varepsilon_b}$. Second, a maximum at the point $p_c = \frac{3m_e^2}{2\varepsilon_b}$. Now we are able to divide the curve in figure 2.3 into three regions:

- Region $\lambda > f(p_c)$: For this case, the solution does not exist and consequently there is no threshold for ultra-high energy photon to annihilate.
- Region between $\lambda < f(p_c)$ and $\lambda = 0$: In this case, we have two different solutions for our relation 2.20. The smaller one represents a lower threshold, whereas the other one takes the role of an upper threshold. This means that there is an interval where background photons are not transparent to ultra-high energy photons and the annihilation to form an electron-positron pair occurs. On the contrary, when the energy of ultra-high energy photons exceeds the upper threshold the absorption by the background photon is not allowed. It is necessary to emphasize the curve behavior at $\lambda = 0$: It correctly describes the standard case without vacuum dispersion, where the upper threshold tends to $+\infty$.
- Region $\lambda < 0$: This region is similar to the standard case in special relativity with only one lower threshold. The difference originates in the reduction of the threshold, since $p < p_0$.

The difference between our resulting modified threshold relation and the one derived in the work of Li & Ma (2021) originate in the use of different dispersion relations. In their analysis, they applied a dispersion relation in the following form:

$$\omega^2 = k^2 - \xi k^n, \tag{2.21}$$

where they fixed n = 3. In this case, the role of ξ is the same as λ figuring in our dispersion relation and we also assume $k \sim p$. Their resulting equation for modified threshold relation is given as:

$$\xi = \frac{4\varepsilon_b}{k^{n-1}} - \frac{4m_e^2}{k^n}, \tag{2.22}$$

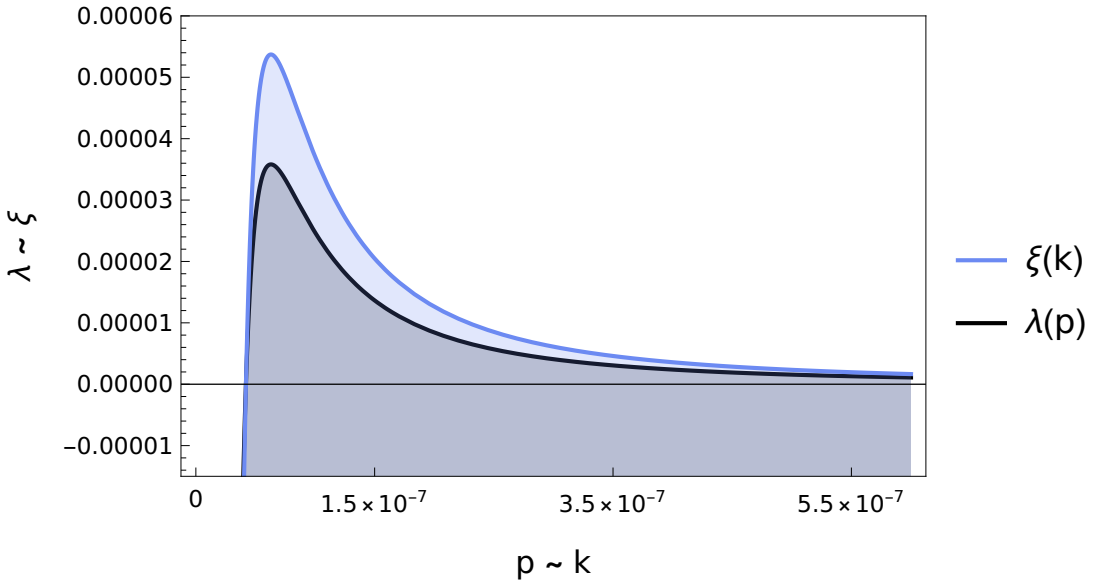

Figure 2.4: Comparison of the two modified threshold relations using two different dispersion relations 2.22 and 2.20. The only difference between the two curves is in the prefactor.

for $k > 0$. The comparison of the two resulting dependencies is illustrated in figure 2.4. As we can see, the curve behavior is in both cases the same, as well as the values of the points intersecting the x-axis and the maximum points. The only difference between equations 2.22 and 2.20 is in the prefactor.

2.3 Numerical approach to modified threshold relation

The relation 2.20 derived in the previous subsection represents a simplified approximate solution because of the Taylor expansions with the neglect of higher degrees. To obtain a more precise solution for our λ dependence, we applied a numerical approach using Wolfram Mathematica Language.

From now on, we take λ as a parameter and ask what is its potential value for photons approaching the Planck scale. Firstly, we determined the value of parameter λ for a concrete value of momentum p from the relation 2.18, where we substituted H_0 with the 2.16 expression. We continued with defining the function of the following form:

$$4m_e^2 = \frac{4}{\lambda^2}\left(1-\sqrt{1-\frac{\lambda p}{1+\lambda p}}\right)^2 + 2\varepsilon_b\left(\frac{2}{\lambda}\left(1-\sqrt{1-\frac{\lambda p}{1+\lambda p}}\right)+p\right)-p^2, \quad (2.23)$$

that takes a p value and outputs the resulting λ value. We made a table with 600 pairs of evaluated λ values for the p values of the same interval as is presented on the x-axis in figure 2.3. Eventually, we plotted the resulting pairs on a graph. The result is illustrated in figure 2.5. We also plotted both numerical and approximative solutions on the same graph (figure 2.6). In this case, we see the approximative curve fitted nicely the numerically evaluated pairs of λ and p. Finally, we did the numerical solution for the $\xi(k)$ dependence of Li & Ma (2021) to compare with our $\lambda(p)$ dependence. The result is shown in figure 2.7.

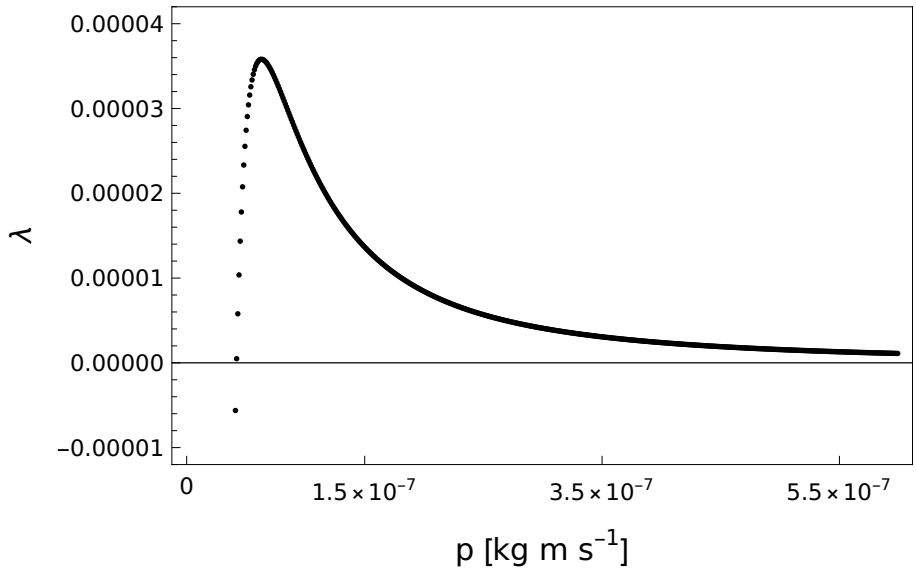

Figure 2.5: Modified threshold relation derived using the numerical approach. The shape of the resulting curve is identical to the one in figure 2.3.

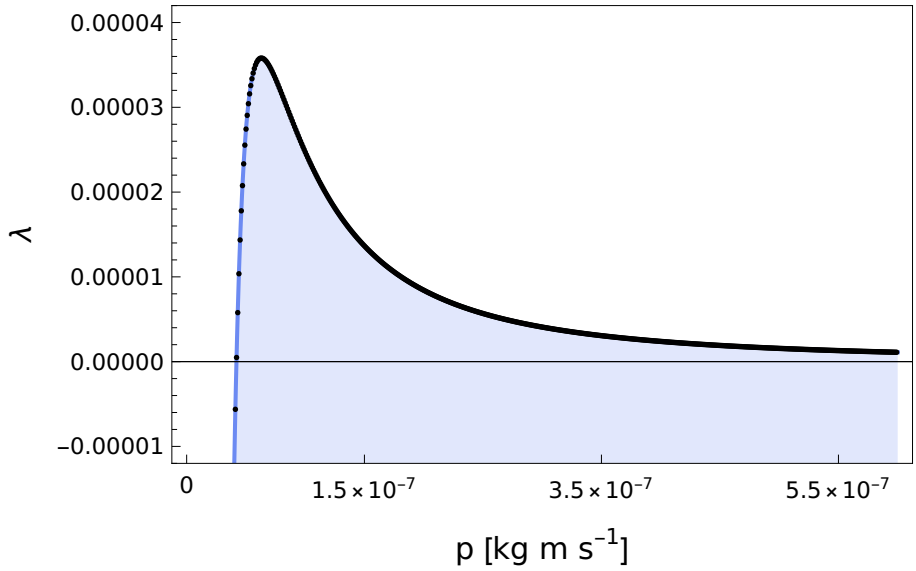

Figure 2.6: Comparison of both approximate and numerical solutions. In this case, the curve from the approximate solution (blue) fitted nicely the pairs of λ and p found by numerical solving (black).

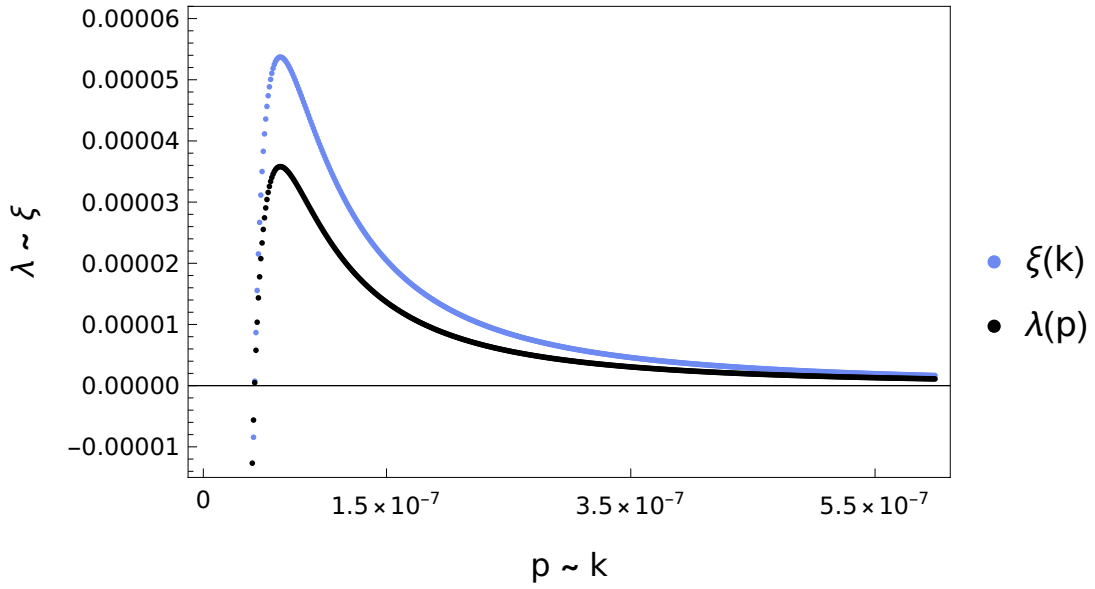

Figure 2.7: Comparison of both numerical solutions for our $\lambda(p)$ and $\xi(k)$ from work of Li & Ma (2021). Shapes of the curves follow the same appearance as in figure 2.4.

In-vacuo dispersion

3.4 Arrival-time difference formulas

Another of the observable consequences of quantum gravity theory with its deformation of the Lorentz invariance is the in-vacuo dispersion effect. Due to the granular structure of space-time, it acts as a dispersive medium for particle propagation through the universe. This causes the energy dependence of the velocity of particles — two simultaneously emitted photons of different energies from a source should be detected by terrestrial detectors at different times (Ronco et al., 2022). The value of the time delay between two emitted photons of different energies is usually miniature, but it can accumulate when the photons propagate cosmological distances. For instance, if we try to manage the experiment on Earth with photons of TeV energies and distances of thousand kilometers, the time of arrival delays would be in the orders of $\sim 10^{-18}$ seconds (Amelino-Camelia, 2013). This is why gamma-ray bursts present the best tool for investigating the in-vacuo dispersion effect. They are capable to accumulate a minuscule effect thanks to their enormous distances and at the same time, they possess immense energy that approaches the Planck energy scale.

From the modified dispersion relation presented in 1.8, we are able to obtain a velocity law, a relation describing the energy dependence of the speed of photons (Amelino-Camelia et al., 1998; Amelino-Camelia, 2013):

$$v \simeq 1 - \frac{m^2}{2E^2} + \eta \frac{n+1}{2} \frac{E^n}{E_{\mathrm{Pl}}^n}, \tag{3.24}$$

if we assume the velocity description as $v = dE/dp$. Using the equation 3.24, Amelino-Camelia (2013) in his work derived the resulting relation for the momentum-dependent difference of arrival time between two particles of different energies:

$$\Delta t \simeq \eta \frac{n+1}{2H_0} \frac{p^n}{E_{\mathrm{Pl}}^n} \int_0^z dz' \frac{(1+z')^n}{\sqrt{\Omega_m (1+z')^3 + \Omega_\Lambda}}, \tag{3.25}$$

where Ω_m, Ω_Λ, H_0 are cosmological parameters, E_{Pl} is the Planck energy and the distance is expressed via integration through redshift. For the linear modification scenario, we assume $n = 1$, meaning the energy and time of arrival difference should follow the linear correlation. The Greek letter η has either a value of 1 if we consider the subluminal case of propagation — photons of higher energies propagate slower than low-energy photons, or a value of -1 for the superluminal case — higher energy photons propagate faster than lower energy photons. In our thesis, we will be working only with the subluminal case.

For redshifts smaller than 1, the time delay at arrival between two photons with energy difference ΔE acquires the following simplified form (Amelino-Camelia & Smolin, 2009):

$$\Delta t|_{\text{small}-z} \simeq \eta \frac{\Delta E}{E_{\text{Pl}}} L, \tag{3.26}$$

where $L = \frac{z}{H_0}$ is the distance of the photon source.

The intensity of the in-vacuo dispersion was investigated in multiple studies, analysing the detections of the brightest gamma-ray bursts. Unfortunately, the study of such phenomena is limited by the very few high-energetic events for which the in-vacuo dispersion should become conspicuous. One of these detections, a gamma-ray burst from October 9, 2022 (described more precisely in the section 4.2) was analysed in the work of Zhu & Ma (2022). They adopted a formula presented in 3.25, and provided a calculation for the time delay between low-energy photons (less than 1 MeV) and an ultra-high energy photon of 99.3 GeV emitted at the same time as low-energy photons. They calculated the resulting time delay as 19.8 seconds. While comparing the data from the Fermi LAT Telescope and its corresponding light curves for multiple energy bands, they observed a significant sharp spike of low-energy photons, detected around ~ 20 seconds before the 99.3 GeV photon event, meaning the spike could present a possible evidence of the in-vacuo dispersion. Similarly in our work, we will investigate the most energetic events detected by current telescopes and try to discover the temporal differences between the peaks of signals. Our analysis is described in detail in the following chapter.

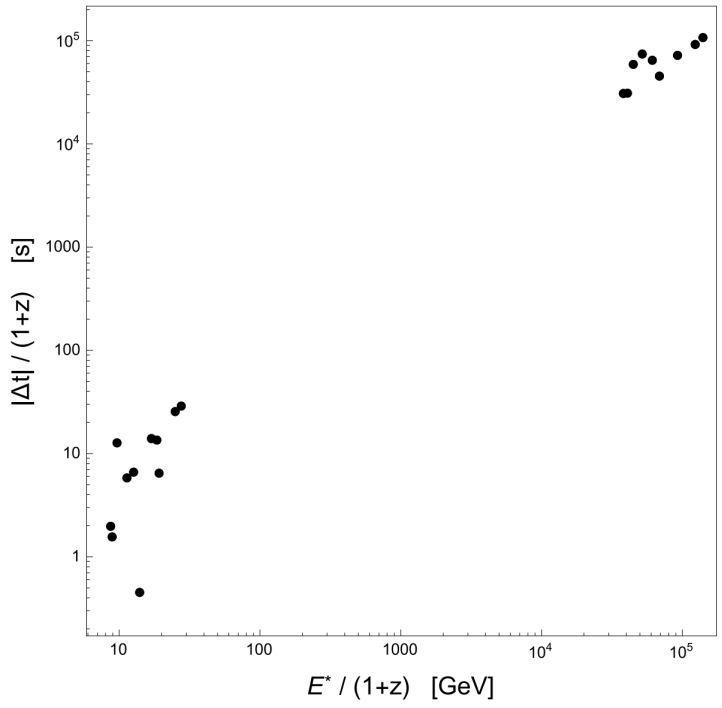

Figure 3.8: Statistical analysis of high-energy photons (left corner) and neutrinos (right corner) from multiple gamma-ray bursts was presented in the work of Amelino-Camelia et al. (2017). They adopted a modified 3.25 relation and calculated the resulting time delays at the maximal energies of the bursts, figuring out that there is a significant correlation between the photon and neutrino features.

Data analysis process

4.1 GRB detectors

The study of threshold anomalies requires mainly the theoretical apparatus of physics. Subsequently, in the practical analysis, we will restrict ourselves only to the study of the most energetic gamma-ray bursts ever observed by humankind, for which the possibility of their observation is extremely rare, and the explanation of such bursts is the most suitably described by the quantum gravity theory with its modified threshold approach. Having this condition for the gamma-ray bursts clarified, we will mainly focus during the data analysis on the observation of in-vacuo dispersion.

The Earth's orbit as well as its surface possesses multiple detectors of gamma-ray bursts. For quantum gravity purposes the main role takes the energy range the detector is able to capture and the temporal resolution. Let us mention some of the currently working facilities:

- The Neil Gehrels Swift Observatory which works in the optical, ultraviolet, X-Ray, and gamma-ray wavebands. It consists of three different instruments among which the Burst Alert Telescope (BAT) has the widest energy range of 15 to 150 keV (Barthelmy et al., 2005). The temporal resolution of the BAT instrument is 100 microseconds [e1].

- The Large High Altitude Air Shower Observatory (LHAASO) which is situated in Daocheng, Sichuan province of China, and includes electromagnetic particle detectors, muon detectors, water Cherenkov detector array, and a wide field-of-view air Cherenkov telescopes. This gamma-ray astronomical observatory operates in the energy range between 100 GeV and 1 PeV with the temporal resolution in nanoseconds (Cao et al., 2019).

- The Fermi Gamma-ray Space Telescope which operates in the gamma-ray area. The main components are the Large Area Telescope (LAT) and the Gamma-ray Burst Monitor (GBM). These two detectors together are able to cover the energy range from 8 keV to 300 GeV. The temporal resolution for GBM is 2 microseconds (Thompson & Wilson-Hodge, 2022).

- International Gamma-ray Astrophysics Laboratory (INTEGRAL), composed of four scientific instruments — the SPI spectrometer, IBIS imager, JEM-X X-Ray monitor, and the OMC optical monitoring camera. They operate in the energy range between 15 keV to 10 MeV. SPI, the main instrument of the laboratory possesses the absolute timing precision of 50 microseconds (Kuulkers et al., 2021).

- GRBAlpha, which represents the smallest astrophysical space observatory. It covers the energy range from 70 keV to 890 keV, with the time stamping in seconds (Pál et al., 2023).

There are many other facilities working on the observation of gamma-ray bursts, except for the ones listed above. During our data analysis, besides the investigation of the observability of the in-vacuo dispersion effect, we also want to take a look at factors specific to small satellites that affect and complicate the observation of minuscule effects such as dispersion in-vacuo. Taking this ambitious goal into account, we decided to retrieve data from GRBAlpha.

4.1.1 GRBAlpha

GRBAlpha, launched on March 22, 2021, by a Soyuz rocket from Baikonur (Pál et al., 2020), is 1U sized CubeSat designed for detecting and studying gamma-ray bursts. Situated at low Earth orbit (LEO), GRBAlpha also informs about the influence of background at LEO. This mission represents an international project of the Czech Republic, Slovakia, Hungary, and Japan. The nanosatellite has a size of a cube with dimensions of approximately $10 \times 10 \times 11$ centimeters and weighs 1.2 kilograms (Pál et al., 2023).

The main part of the detector is a thallium-activated cesium-iodine crystal of a size $75 \times 75 \times 5$ millimeters. This scintillator is enveloped with an Enhanced Specular Reflector (ESR), which basically plays a role of a reflective foil. A small non-wrapped area of the scintillator possesses a linear array of multi-pixel photon counters (MPPCs), mounted on a printed circuit board (PCB) of size 60×5 millimeters. The scintillator is enveloped again with the black Tedlar layer (DuPont TCC15BL3) and protected with the lead-alloy shielding (PbSb3) on the side of the multi-pixel photon counters (Pál et al., 2023).

The output signal of the biased MPPCs travels to an analog signal chain with the resistor-capacitor networks. The resulting widened pulse is sampled by the analog-digital converter (ADC). The signal then flows through the field-programmable gate array (FPGA) and is handled by the main microcontroller unit (MCU), from which the data stream ends in the radio downlink and is received by two stations in Piszkéstető Observatory in Hungary and in Jablonec in Slovakia (Pál et al., 2023). The resulting data can be downloaded by the scientific community in *.json* and *.txt* formats. The data contains information about the time in the form of the Unix time and UTC, as well as information about the position of the satellite in the form of longitude, latitude, and altitude. The exposure was previously set to 4 seconds, newly the time bins were improved to 1 second. GRBAlpha provides information about the energy range in the interval from 70 keV to 890 keV, divided into 4 or 16 energy channels.

We retrieved multiple data from the GRBAlpha's server, where all the daily detections are stored. Before all else, we wanted to take a look on a casual data without a detection of the gamma-ray burst to know how the count rate is behaving. We decided to pick the data from November 10, 2022. The corresponding graph is illustrated in figure 4.2.

As we can see, even with no gamma-ray burst observed on this day, GRBAlpha detected strong signals when passing through certain areas on the globe. These undesirable detections must be taken into account during the analysis of the gamma-ray burst detections.

Observed signals are mainly caused by the following phenomenons:

- The Van Allen radiation belts — correspond to outer and inner radiation belts composed of high-energy electrons and ions (mostly protons). They are located in the inner magnetosphere of Earth where the geomagnetic field can be approximated as a magnetic field of a magnetic dipole (Koskinen & Kilpua, 2022). GRBAlpha, orbiting the low Earth orbit, pass through the Van Allen radiation belts near the North and South pole of the Earth.
- The South Atlantic Anomaly — this anomaly represents an area from the southern tip of Africa to South America where the Earth's magnetic field is the weakest, only about 22 µT (Koskinen & Kilpua, 2022). Consequently, the satellites passing through this region are exposed to a much higher flux of ionising radiation than usual.

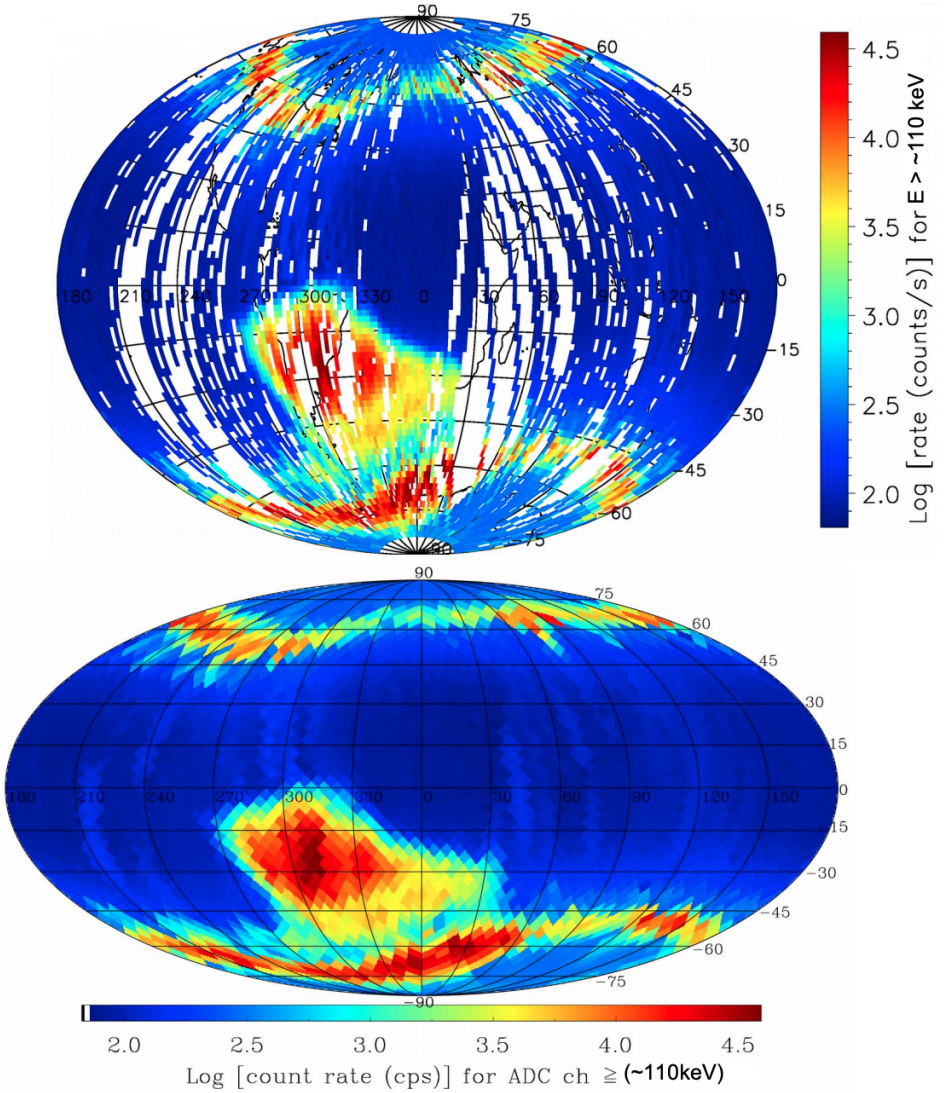

Figure 4.1: The background map at low Earth orbit for E $\gtrsim$ 110 keV. Red parts present the areas with higher concentrations of charged background particles [e2].

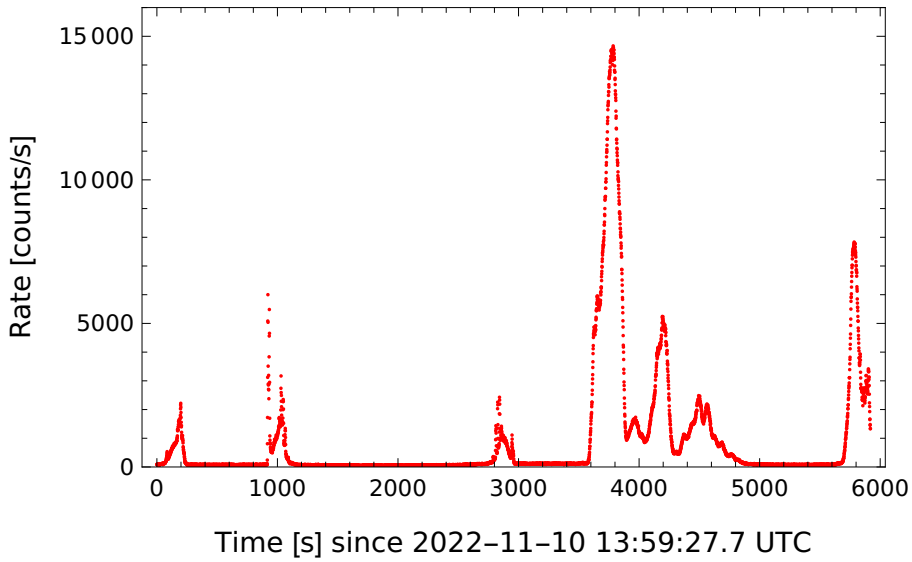

Figure 4.2: GRBAlpha measurement for E $\simeq$ 240 keV from November 10, 2022. The count rate is caused by the satellite's flyover above the areas denoted in figure 4.1.

4.2 Data analysis for GRB 221009A

GRB 221009A was an extraordinarily bright long-duration gamma-ray burst, detected on October 9, 2022, at 13:16:59.99 UT. The burst was located at a right ascension of 288.28 degrees and declination of 19.49 degrees (J2000) (Pillera et al., 2022), in the constellation Sagitta. The redshift was estimated to be z = 0.1505 (Castro-Tirado et al., 2022). This cosmological burst was detected by multiple facilities. Firstly the detection was announced by Fermi Gamma-ray Burst Monitor (Veres et al., 2022) and by the Fermi's Large Area Telescope (Pillera et al., 2022). A nanosatellite GRBAlpha also detected this exceptional burst without saturation (Ripa et al., 2023). The Large High Altitude Air Shower Observatory announced detected photons reaching 18 TeV (Huang et al., 2022), and the Russian air-shower array Carpet-2, located at Baksan Neutrino Observatory, reported a single photon reaching 251 TeV (Dzhappuev et al., 2022). Subsequently, GRB 221009A is now considered the brightest burst ever observed since the beginning of human civilisation and was named as the *BOAT* (Brightest Of All Time) (Burns et al., 2023).

Data from October 9, 2022, were retrieved from GRBAlpha's data server. On this day the time stamping was set to 4 seconds with 16 energy channels operating. We found out that the low energy threshold was set to $\sim$ 80 keV, making the first 3 energy bands unsuitable for analysis because of the high rate of the dark noise. Raw data for one of the energy bands (155 keV) is illustrated in figure 4.3. On this graph, we marked with blue color the area corresponding to the detection of GRB 221009A. A non-zero count rate marked with red color represents the signal detected when GRBAlpha was passing through the regions denoted in figure 4.1. The burst itself is in figure 4.5. We also need to highlight above which part of the globe the satellite was situated in during the detection of such a burst. From figure 4.4 is evident that GRBAlpha was passing through the North Pole, detecting the final part of GRB when transiting the outer Van Allen radiation belt.

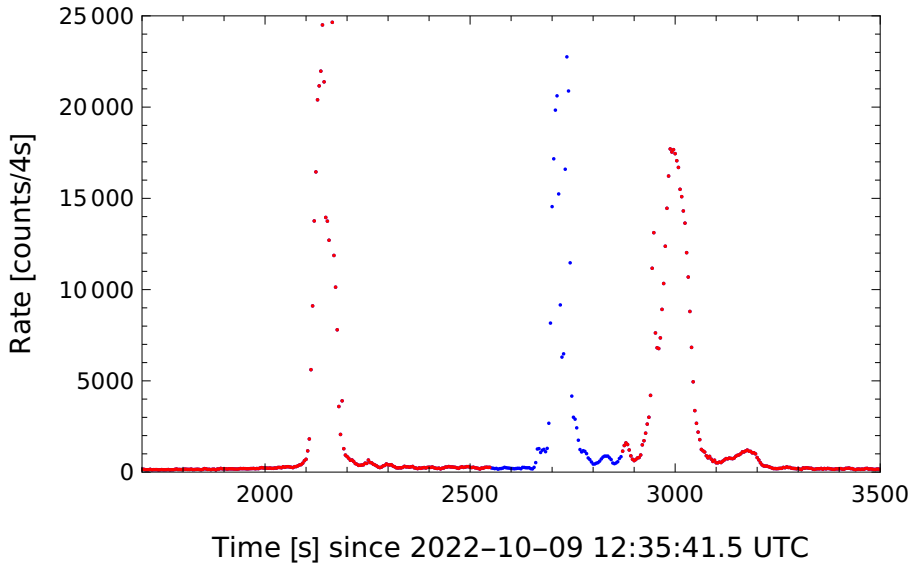

Figure 4.3: Raw data for E $\simeq$ 155 keV from October 9, 2022. We restrict ourselves to the blue part presenting the GRB 221009A.

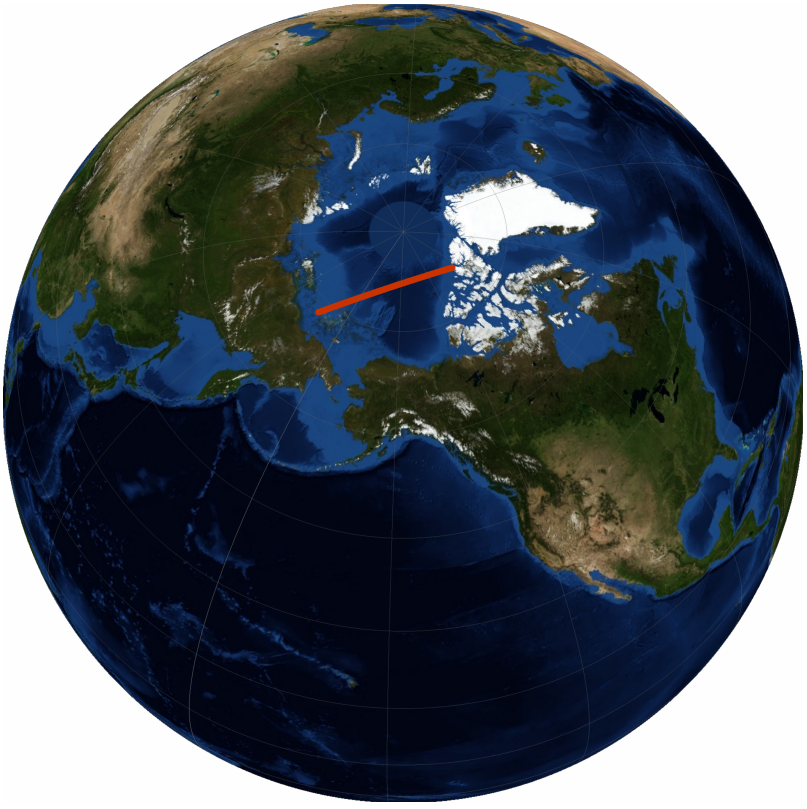

Figure 4.4: Position of GRBAlpha (red) during the detection of GRB 221009A. The satellite was situated on the North Pole, heading to the outer Van Allen radiation belt.

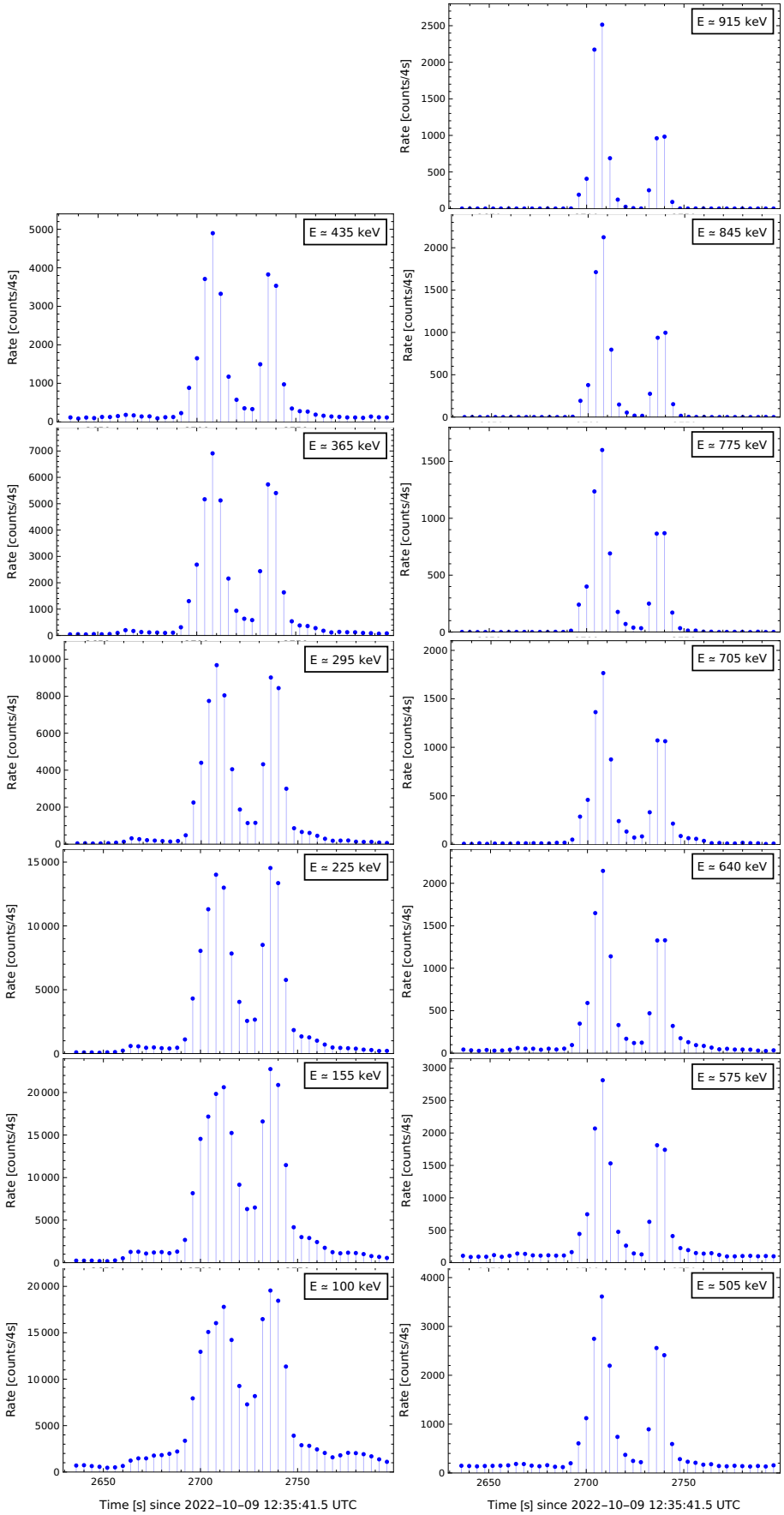

Figure 4.5: Detection of GRB 221009A by GRBAlpha for all 13 energy bands. The first 3 energy bands were automatically set to zero because of the low energy threshold.

The main goal of this analysis is to observe the in-vacuo dispersion effect — a potential time delay between simultaneously emitted photons of different energies. Generally applies the higher the energy of the detected photon is, the greater should be the observed time delay between this and the less energetic photon. In data, this phenomenon should be seen as a very tiny shift of the detected peaks for higher energy ranges. For the position determination of the peaks in all energy bands, we use the Gaussian distribution as follows:

$$f(x;\mu,\sigma) = Ae^{-\frac{(x-\mu)^2}{2\sigma^2}}, \tag{4.27}$$

where A is the normalisation constant of a Gaussian function, μ is the mean value of the distribution we search for, and σ is the standard deviation. Taking into account the appearance of the data in figure 4.5, the objective is to fit both peaks for all energy bands with two Gaussian functions and determine their mean values. Resulting Gaussian parameters μ are summarized in the table 4.1. GRB 221009A data with its fitted Gaussian models are illustrated in figure 4.8.

Table 4.1: Gaussian parameters μ with their errors for both peaks of GRB 221009A detected by GRBAlpha. It is apparent that the μ values evolve with increasing energy.

Energy band [keV]	μ_1 [s]	$\mu_{1,\mathrm{err}}$ [s]	μ_2 [s]	$\mu_{2,\mathrm{err}}$ [s]
100	2709.23	0.381521	2736.77	0.484064
155	2708.86	0.235676	2737.13	0.265058
225	2708.28	0.151369	2737.34	0.155963
295	2707.95	0.120615	2737.54	0.115343
365	2707.74	0.132807	2737.61	0.115007
435	2707.52	0.171647	2737.59	0.148048
505	2707.32	0.221323	2737.69	0.225487
575	2707.26	0.205141	2737.73	0.227955
640	2707.10	0.149616	2737.82	0.169971
705	2707.01	0.123876	2737.82	0.092784
775	2706.85	0.108753	2737.88	0.0440987
845	2706.75	0.0603182	2737.96	0.0620668
915	2706.42	0.0472161	2737.88	0.0641405

After a successful determination of the peak positions, we plot the resulting μ values as a function of energy (figures 4.6 and 4.7). We expect one of the following features in the curve behaviors:

- The curve has a very light increasing character as a result of the in-vacuo dispersion effect. Ultra-high energy photons propagate slower through space because of the quantum space-time structure, causing the visible time delay at arrival.
- The curve has an increasing or decreasing character as a result of the different influences — the ongoing processes at the source of the GRB causing some of the photons to leave the source later, the efficiency and the precision of the detector at different energy ranges, or simply the influence of the background.

- The curve has a nearly constant μ value, which is the outcome of a negligible influence of the quantum gravity effect, nor the influence of the behavior at the source of GRB or of the detector and background.

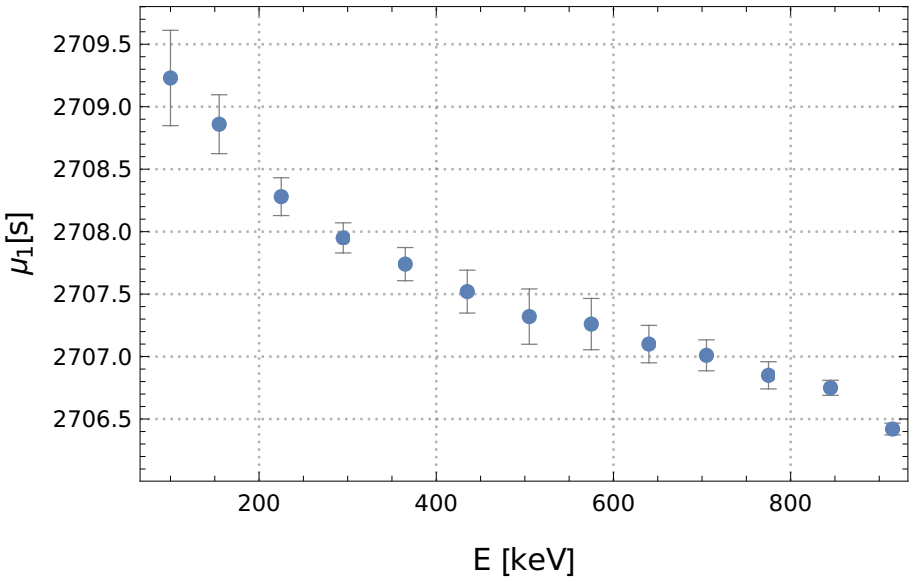

Figure 4.6: Evolution of the μ_1 value of the first GRB 221009A peak with the increasing energy. The decreasing trend of the resulting plot excludes at first glance the influence of the in-vacuo dispersion effect.

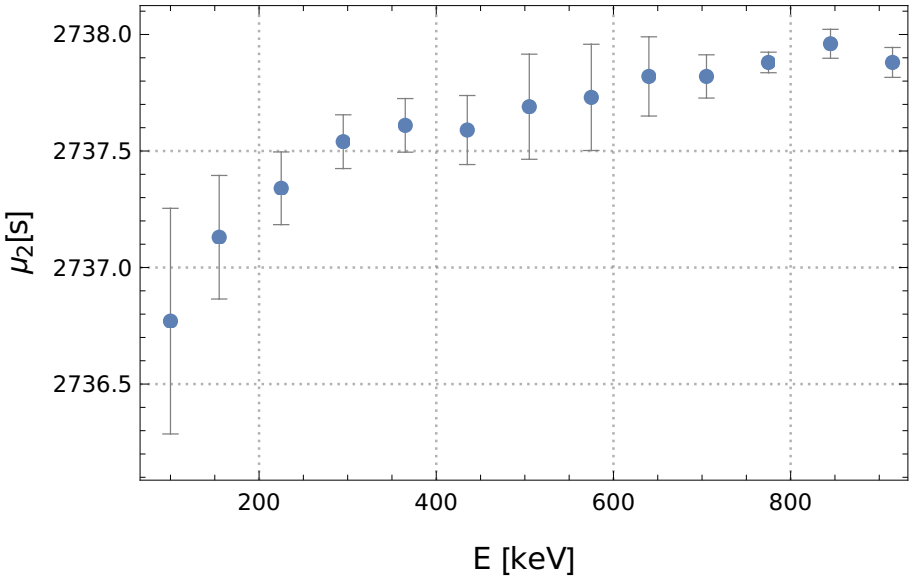

Figure 4.7: Evolution of the μ_2 value of the second GRB 221009A peak with the increasing energy. In this case, the increasing character of the plot can be the result of multiple effects. All of the possible explanations including the observability of the in-vacuo dispersion are discussed in the following chapter.

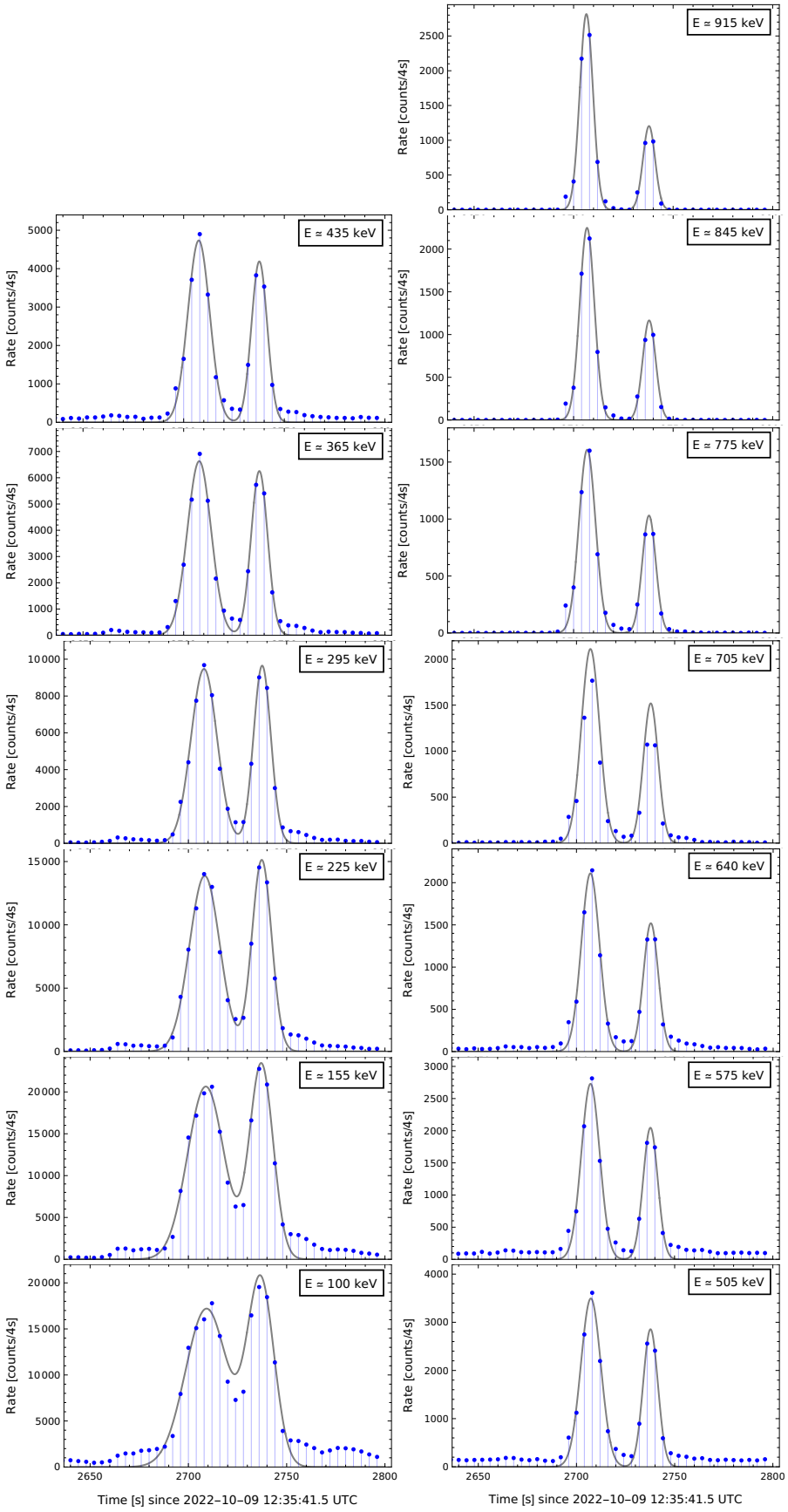

Figure 4.8: GRB 221009A data (blue) for all 13 energy bands fitted by the two Gaussian functions described by the relation 4.27 (grey).

Lastly, we want to take a look at which time bin the maximal count rate was detected for both signals in each energy band, to see the evolution of the maximal count rate with increasing energy. For that, we determine the corresponding time values for occurred maximums for both of the signals. The result is shown in table 4.2. In the case of the first signal, the maximal count rate moved with the increasing energy to an earlier time bin. On the other hand, the second signal reached its maximum for higher energies in the following bin at a later time. Both results are therefore in accord with the resulting dependencies in figures 4.6 and 4.7 determined by a more precise Gaussian fit.

Table 4.2: Determined time bins for each of the 13 energy bands at which the maximal count rate occurred. In both cases, the maximum is moved by one bin for higher energies (each bin is 4 seconds wide).

Energy band [keV]	$t_{1,\max}$ [s]	$t_{2,\max}$ [s]
100	2712	2736
155	2712	2736
225	2708	2736
295	2708	2736
365	2708	2736
435	2708	2736
505	2708	2736
575	2708	2736
640	2708	2740
705	2708	2736
775	2708	2740
845	2708	2740
915	2708	2740

4.3 Data analysis for GRB 230307A

GRB 230307A was a very bright long-duration gamma-ray burst, first detected by Fermi GBM on March 7, 2023, at 15:44:06 UT (Fermi GBM Team, 2023). Fermi GBM also estimated its location at right ascension of 54.1 degrees and declination of -76.6 degrees (J2000). The detection was later announced by GECAM-B observatory (Xiong et al., 2023), italian AGILE/MCAL (Casentini et al., 2023), AstroSat CZTI (Navaneeth et al., 2023) and many others. The redshift was estimated to be z = 0.065 thanks to the H α, N II, and S II emission lines (Gillanders et al., 2023). GRB230307A was also detected by GRBAlpha, where the peak count rate reached almost 10 000 counts per second (Dafcikova et al., 2023). Consequently, GRB 230307A is now considered the second brightest gamma-ray burst ever observed after GRB 221009A.

Once again we retrieved the data from March 7, 2023, from GRBAlpha's data server. The exposure time was set to 1 second with 4 energy bands operating, covering the whole energy range of the detector. A sample of the GRB230307A detection data with the most

important columns for our analysis can be found in tables 1.6 and 1.7 in Appendix. Raw data for E $\simeq$ 240 keV is illustrated in figure 4.10, where the blue part represents the GRB 230307A and the red non-zero area is the influence of the background particles. From the position of GRBAlpha above the globe during the detection of such a burst (figure 4.11) is evident that the satellite was situated in the Indian Ocean, heading to the South Pole and entering the outer Van Allen radiation belt at the tail part of the burst. Raw data of the burst is illustrated for all 4 energy bands in figure 4.9.

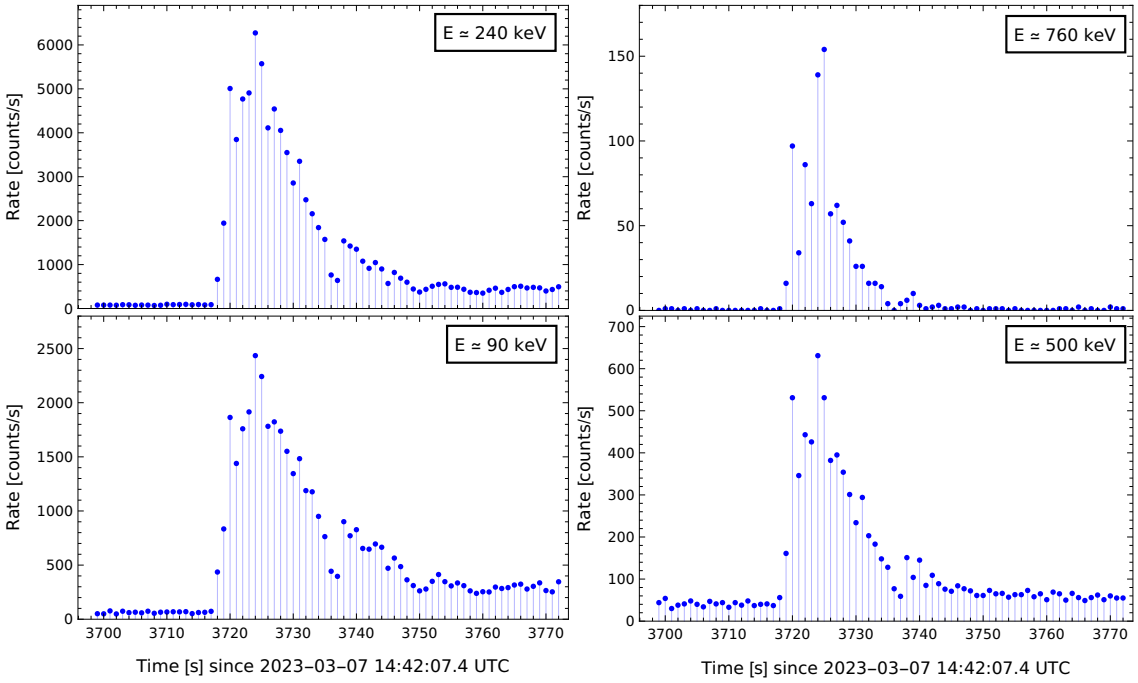

Figure 4.9: Detection of GRB 230307A by GRBAlpha for all 4 energy bands covering the whole energy range of the detector.

We adopt an analogous approach to the GRB 230307A data analysis as in the previous subsection 4.2. In this case, we will fit the corresponding datasets only with one Gaussian distribution (described by the relation 4.27) for every energy band, as is evident from the data appearance the figure 4.9. The resulting μ values with their errors are listed for every energy band in table 4.3. Corresponding fits for GRB 230307A data are illustrated in figure 4.12. The temporal evolution of the peak with increasing energy is in figure 4.13.

Table 4.3: Gaussian parameters μ with their errors for the only peak of GRB 230307A. In this case, the peak is also evolving with increasing energy.

Energy band [keV]	μ [s]	μ_{err} [s]
90	3726.79	0.483586
240	3725.49	0.318954
500	3725.06	0.375299
760	3724.31	0.238166

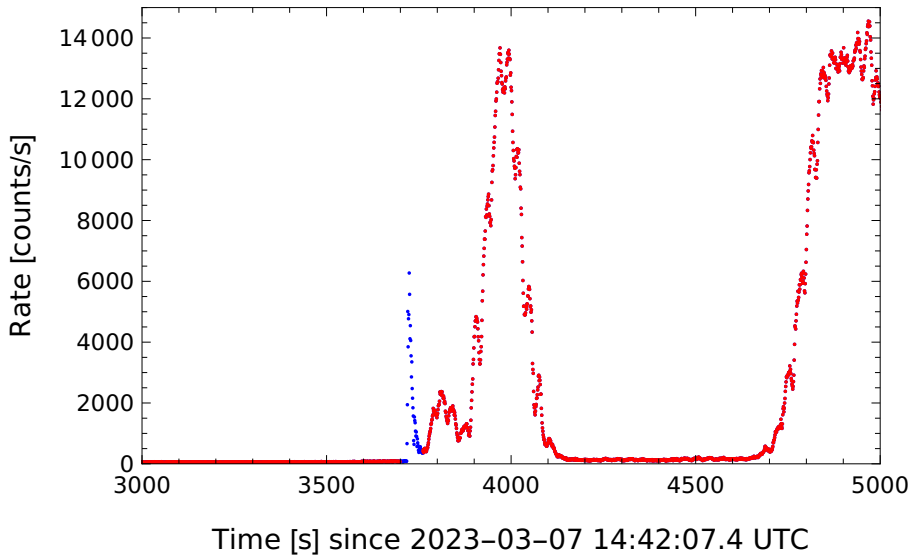

Figure 4.10: Raw data for E $\simeq$ 240 keV from March 7, 2023. We restrict ourselves to the blue part presenting the GRB 230307A.

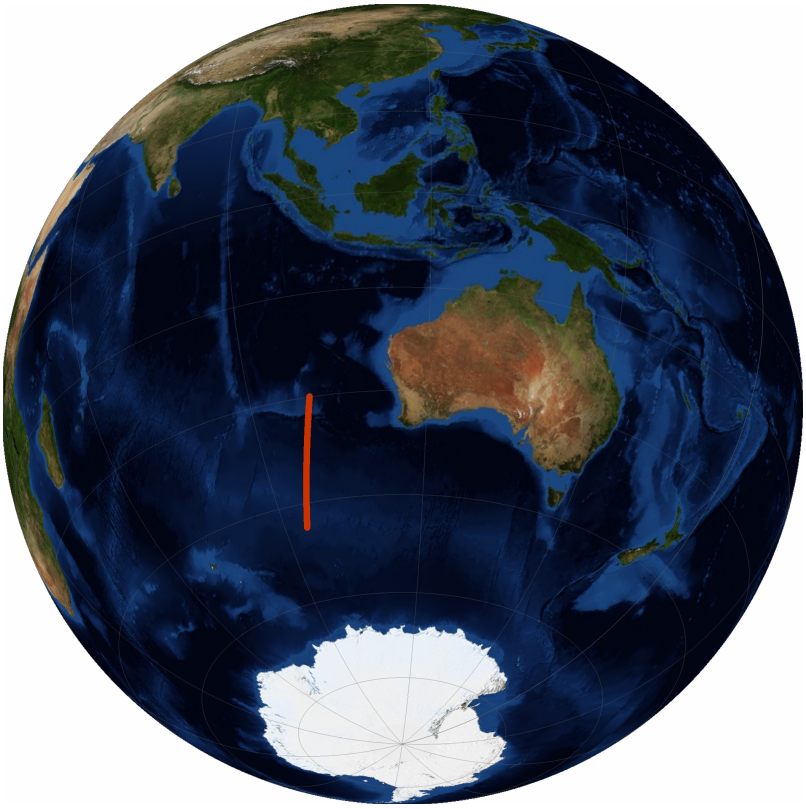

Figure 4.11: Position of GRBAlpha (red) during the detection of GRB 230307A. The satellite was situated in the Indian Ocean, heading to the South Pole and entering the outer Van Allen radiation belt at the final part of the burst.

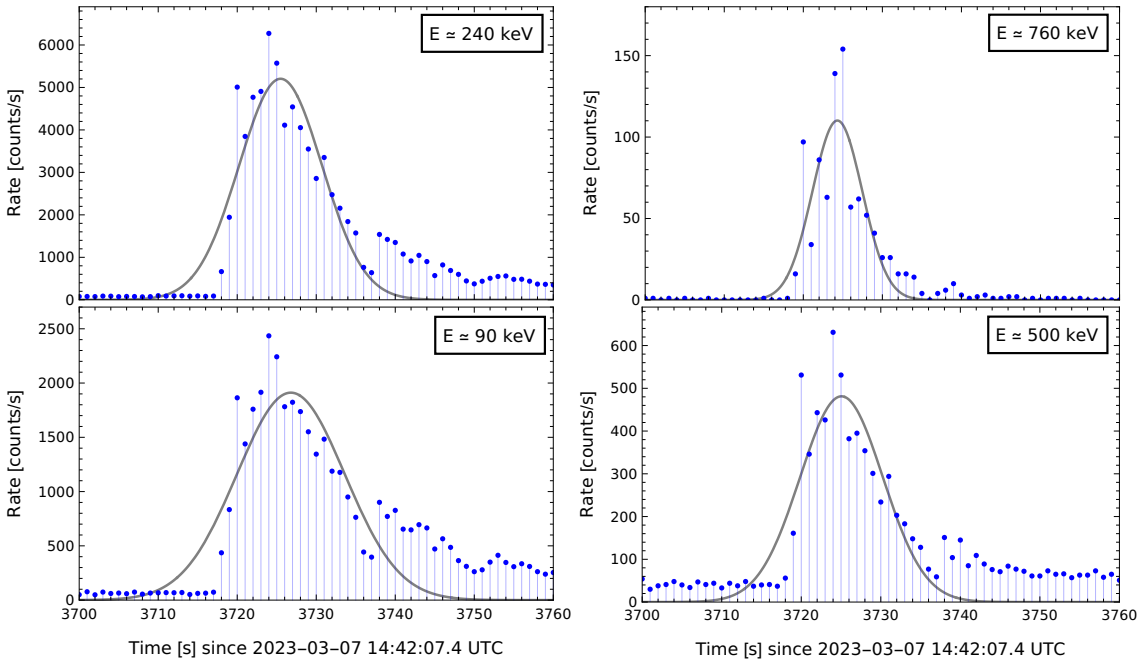

Figure 4.12: GRB 230307A data (blue) for all 4 energy bands fitted by the Gaussian function described by the relation 4.27 (grey). In contrast to the previous gamma-ray burst data, in this case, the Gaussian curve appears to be less precise.

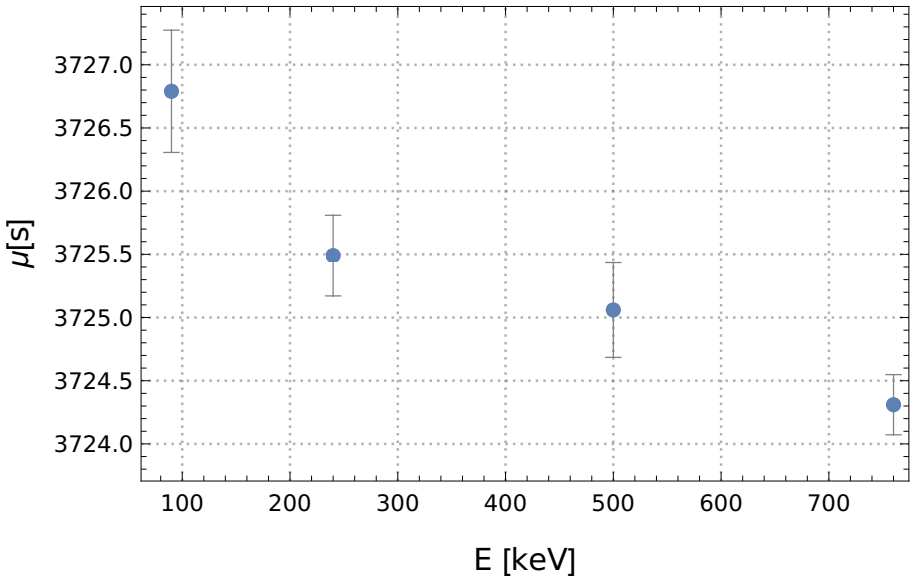

Figure 4.13: Evolution of the μ value of the GRB 230307A peak with increasing energy. Similarly to figure 4.6, this case also does not confirm the in-vacuo dispersion effect.

Lastly, we want to take a look at which time bin the maximal count rate was detected in each of the 4 energy bands, to see the potential evolution of the maximal count rate with increasing energy. The result is shown in table 4.4. In this case, the maximal count rate moved to the following time bin in the last, most energetic energy band. This observation

does not correspond to the result obtained by fitting in figure 4.13, mostly because of the not very conveniently chosen fitting function. Possible explanations for the obtained results and the observability of the in-vacuo dispersion are described in detail in subsections 5.1 and 5.1.1.

Table 4.4: Determined time bins for each of the 4 energy bands at which the maximal count rate occurred. The maximum value moved to the following time bin in the highest energy band (each bin is 1 second wide).

Energy band [keV]	$t_{\max}$ [s]
90	3724
240	3724
500	3724
760	3725

Interpretation of results

5.1 Observability of the in-vacuo dispersion

Whereas the redshifts for both gamma-ray bursts analysed in the sections 4.2 and 4.3 are smaller than 1, we utilise for the calculation of the resulting time-of-arrival delay of photons the simplified relation 3.26. Adopting the values of variables performing in the relation 3.26 as $\eta = 1$ (subluminal case), $\Delta E_1 = 870$ keV (the energy range of the detector for GRB 221009A), $\Delta E_2 = 820$ keV (the energy range of the detector for GRB 230307A), $H_0 = 2.37 \times 10^{-18}$ s^{-1} (the Hubble constant) and E_{Pl} as a value of Planck energy from 1.2, we come to the values of time delays Δt presented in the table 5.5. The E_{QG} in the third column presents what value the Planck energy should have to be able to observe an in-vacuo dispersion with GRBAlpha in the orders of seconds (here we considered the minimal value of the time delay as 5 seconds). It is necessary to emphasize that in the case of GRB 221009A data analysis, the new energy range of the detector was adopted (from 70-890 keV to 80-950 keV) after almost 2 years of GRBAlpha in orbit. For correctness, we use the new ΔE_1 energy range for the Δt determination for GRB 221009A.

Table 5.5: Resulting values of Δt for both analysed gamma-ray bursts. The third column presents the needed value of the Planck energy to observe a potential in-vacuo dispersion effect with GRBAlpha.

Gamma-ray burst	Δt [s]	E_{QG} [eV]
GRB 221009A	4.528×10^{-6}	1.105×10^{22}
GRB 230307A	1.843×10^{-6}	4.498×10^{21}

As we can see, the in-vacuo dispersion phenomenon is impossible to observe with the detectors like GRBAlpha, because the time-of-arrival delays in orders of microseconds are practically unobservable in the datasets with the time stamping in seconds. The upper limit for the quantum gravity energy would have to be $\sim 10^{-7}\, E_{\mathrm{Pl}}$, which is not consistent with the theory of quantum gravity predicting the Lorentz invariance violation in the orders of the Planck energy.

5.1.1 Explanation of the trends

We have figured out that the in-vacuo dispersion effect has zero influence on the position of the detected peaks of the GRBs. Therefore, there must be other phenomenons causing

the behavior of the curves as represented in the figures 4.6, 4.7 and 4.13.

The most suitable explanation for the trends is a spectral lag phenomenon. The spectral lags appear mainly for the long GRBs (time duration $>$ 2 seconds), while short GRBs have a zero spectral lag (Norris et al., 2001). They represent the energy-dependent lags originating at the source of a gamma-ray burst and causing the visible time delay between the photons of different energies. A majority of the long GRBs have positive spectral lags, meaning that the lower energy photons are detected later than the high-energy photons (Norris et al., 2000). On the other hand, observation of negative spectral lags is very exceptional and has been observed only in a few cases (Chen et al., 2005). The width of a GRB signal is also related to the spectral lags phenomenon — it becomes wider for lower energies, as can be observed also in our datasets in the figures 4.5 and 4.9. From analyses of multiple GRBs described in the works of Norris et al. (2000) and Foley et al. (2008) was found the time-of-arrival delay of photons in the orders of *seconds* for energy bands between dozens and hundreds of kilo electronvolts. This calculation supports the idea of a possible explanation of the trends in our figures 4.6 and 4.13 by the positive spectral lag phenomenon. The physical explanation of spectral lags has not yet been discovered and is nowadays a matter of debate in the scientific community, but one of the possible explanations is presented by the internal shock model (Foley et al., 2008) — a plasma dispersion which causes the slowdown of the particles of lower energies. Moreover, when we search for the GRB 221009A detections from other satellites, e.g. the Konus-Wind detection (Frederiks et al., 2023), we find a similar case of the energy peaks evolving with time. Subsequently, spectral evolution represents a very promising explanation of the decreasing behavior of curves.

The increasing trend in figure 4.7 but as well the other two figures with decreasing trends can be explained also by other effects. One of them can be the inconsistency in the sensitivity of the GRBAlpha detector for different energies, as well as the precession rotation with the $\sim$ 47 second frequency of the detector visible in the background for lower energy bands when approaching poles (Ripa et al., 2023). A big impact on the temporal evolution of the second peak of GRB 221009A can also have the fact that the satellite was situated on the North Pole, and could possibly detect the unwanted particles that affected the measurement. The wobble of GRBAlpha becomes significant at these latitudes, supporting the fact that approaching radiation belts and the wobble of the satellite could be the most proper explanations for the increasing curve behavior in figure 4.7.

Besides our discovery of the increasing tendency of the peak positions in figure 4.7, the later arrival of the high-energy photons in comparison with the lower energy photons was observed in multiple studied gamma-ray bursts in the past (e.g. GRB 090510 (Ackermann et al., 2010), GRB 080916C (Abdo et al., 2009)). It is important to say that in none of the gamma-ray detections yet we were able to exclude other physical explanations of the time delay effect and insist on the in-vacuo dispersion feature. We stress that the papers investigating both of the mentioned gamma-ray bursts concluded with the statement that the in-vacuo dispersion manifestation is highly implausible (Abdo et al., 2009). Therefore, our work contributed to the knowledge of in-vacuo dispersion with the samples of secondary effects we must consider when investigating in-vacuo dispersion in the near future.

5.2 Other explanations for the GRB 221009A detection

Observation of a gamma-ray burst of such high energies is practically impossible according to the standard model of physics. The probability of surviving for 18 TeV photons is approximately 10^{-7}(Franceschini & Rodighiero, 2017). Consequently, this exceptional detection opens the door for new ambitious theories. Except for the quantum gravity theory, a few other theories are trying to explain the *BOAT* detection. Let us mention some of them:

- Sterile/Heavy Neutrino: The hypothesis predicts the existence of an active neutrino connected with photons originating in the gamma-ray burst. Thanks to the dipole interaction or mixing, they are able to transform into sterile/heavy neutrinos. Due to this conversion, the sterile/heavy neutrino travels long distances across space-time without being attenuated by the low-energy background photons. When approaching the Earth, they convert back into active neutrinos and photons and can be easily detected by our terrestrial and orbiting detectors (Cheung, 2022; Guo et al., 2023).

- Axion-like particles: Similarly to sterile/heavy neutrinos, this hypothesis describes the conversion of photons into light pseudoscalar bosons called axion-like particles (ALPs). When a transverse magnetic field is presented, photons transform into ALPs and vice-versa (Massó & Toldrà, 1995). In this form, they propagate cosmological distances without attenuation. Near the Galaxy's magnetic field, some of the ALPs convert back into high-energy photons (Wang & Ma, 2023).

- Standard physics: Standard physical model also might be capable of explaining the GRB 221009A observation. In the work of Zhao et al. (2023), they performed a set of 10^6 Monte Carlo simulations to investigate the probability of the photon surviving during a severe attenuation by low-energy background photons. They assumed the number of detected events is described by the Poisson distribution. The result of the analysis was that standard physics is still capable to observe 18 TeV photons within a 3.5 sigma confidence interval.

5.3 Future of the phenomenological quantum gravity

The idea of studying the quantum structure of space-time using gamma-ray bursts was developed first by Amelino-Camelia and his collaborators almost 30 years ago (Amelino-Camelia et al., 1998). Nowadays, the scientific community strives to launch missions that will focus for the first time among other fields of interest also on the investigation of the quantum gravity effects.

The most ambitious planned mission worth mentioning is the Gamma Ray Astronomy International Laboratory for Quantum Exploration of Space-Time (GrailQuest), which represents a mission consisting of a constellation of hundreds or thousands small satellites. Each instrument should be equipped with an array of crystal-made scintillators and Silicone Drift Detectors (SDDs). Every satellite is expected to be situated in or near low Earth orbit, covering the energy range in the order from a few kilo-electron volts to mega-electron volts

and having an outstanding temporal resolution (from 10 to 100 nanoseconds range) with a wide field of view (Burderi et al., 2021).

The GrailQuest mission will mainly focus on the investigation of three following scientific topics — the investigation of the gamma-ray and hard X-ray temporal variability of the transient events, the exact localisation of bright high-energy transients, and the study of the structure of space-time. With the constellation of small detectors acting as a single detector of exceptional effective area, we will be able to determine precisely the position of the incoming GRB, and subsequently obtain a single lightcurve for each energy band from all of the detectors. The light curves for different energy ranges with a very precise temporal resolution then can be used for measuring the effect of the in-vacuo dispersion and searching for a dispersion law for photons in a vacuum. Therefore, the GrailQuest mission would provide the first experiment to test the quantisation of space-time. This aspirational mission is proposed for a long-term ESA science program, the Voyage 2050 (Burderi et al., 2020).

5.3.1 Mission HERMES

A technologic and scientific pathfinder of GrailQuest that is already under development and is linked also to Masaryk University and its researchers is the mission called HERMES (High Energy Rapid Modular Ensemble of Satellites). This mission consists of six 3U nano-satellites of the shape of parallelepiped and the size of $30 \times 10 \times 10$ centimeters. The advantage of using these nano-satellites as space observatories origins in the fact that we can first launch reduced versions of a mission (the HERMES pathfinders) to prove its function in orbit, test the units, and improve the following launches if needed. Another great advantage is that when one or a few of the satellites stop working, the constellation would still be able to operate (Fiore et al., 2020).

HERMES is designated for studying gamma-ray bursts and other high-energy transients and is distinguished by its excellent temporal resolution in a fraction of microseconds and wide energy band. The detection of photons of energies from 20 keV to 0.5 MeV is provided by a detector situated at the top of the spacecraft in the form of Gadolinium-Aluminum-Gallium Garnet scintillator crystals (GAGGs). GAGGs are arranged in 12 blocks of 5, containing together 60 crystals. In addition, each of these blocks surrounds also the Silicon Drift Detector (SDD) for the detection of photons with energies from 2 to 20 keV (soft X-ray). The sides and bottom of the detector are wrapped in tungsten layers to minimize the cosmic X-ray background (Burderi et al., 2020).

The mission will concentrate (analogically to GrailQuest) on three main scientific topics linked to high-energy transient events — an accurate localisation of gamma-ray bursts, an investigation of a gamma-ray burst inner engine, and a quantum structure of space-time on a minuscule Planck scale. The precise localisation of transient astrophysical sources will be provided thanks to the different positions of the detectors in orbit, causing the delay in the arrival time of a signal for compared detectors. This principle is known as the Temporal Triangulation method. HERMES will also try to answer at least some of the longstanding questions about emission mechanisms during the birth of a gamma-ray burst. The most ambitious of the planned fields of interest is without any doubt the search for a dispersion relation for photons (Fiore et al., 2020). Similar to the results of this thesis, the

observation of in-vacuo dispersion with HERMES is going to be difficult mainly because of the intrinsic delays originating at the source of the emitted photons. However, intrinsic lags do not depend on the distance, making the dependence on energy and redshift a unique feature of quantum gravity helping us to distinguish the in-vacuo dispersion (Burderi et al., 2020).

The launch of the full HERMES Pathfinder constellation of 6 nano-satellites is for now expected in mid-2024 [e4].

Conclusions

The aim of this work was to introduce the quantum gravity theory, a theory seeking to find the approach respecting both quantum mechanics and gravity theory and therefore uncover the true nature of the universe. The principle of this theory originated in the possible modification or even violation of the Lorentz symmetry when reaching the microscopic Planck scale. After the presentation of the modified dispersion relation taking into account the influence of quantum gravity, we investigated the two main hypothetically observable effects having the power to possibly confirm the theory in the future.

The second chapter of the thesis was dedicated to the threshold anomaly phenomenon. We described the case of standard physics, where the ultra-high energy photons cannot propagate through cosmic space because of their severe annihilation with the low-energy background photons. The apparent sign of malfunction of the standard model of physics was brought after the detection of the most energetic GRB 221009A with photons with energies reaching 18 TeV. Therefore, we tried to derive a modified threshold relation that would respect the reappearance of ultra-high energy photons. For that, we used our modified dispersion relation presented in the first chapter and the energy-momentum conservation law presented in another work. We derived firstly the approximative solution using the Taylor series, then we applied also the numerical solving. The result showed us different behavior of the annihilation threshold with different values of the quantum gravity parameter. The resulting relation also correctly described the case of zero value of the quantum gravity parameter (standard physical model).

In the fourth chapter, we conducted an analysis to investigate the potential observability of the in-vacuo dispersion effect. The in-vacuo dispersion predicts the speed dependence on the energy of a photon. Therefore, high-energy photons should propagate slower through space-time in comparison with low-energy photons. The analysis was performed on GRB 221009A and GRB 230307A data from CubeSat GRBAlpha. In the case of the most energetic burst ever observed, GRB 221009A, GRBAlpha detected 2 strong signals in 13 of the 16 energy channels with the 4-second exposition. The first 3 of the 16 energy channels were automatically set to zero due to the set of low energy threshold on ~ 80 keV and a subsequent high rate of the dark noise. GRB 230307A was detected as one wider signal in 4 energy channels with an exposition of 1 second. Every signal in each energy channel was fitted with the Gaussian function. We obtained the resulting mean values of the peak positions for every energy channel from the least energetic to the most energetic. The resulting mean values were plotted on graphs as functions of the energy, to see the evolution of the peak positions with increasing energies.

In the last, fifth chapter, we discussed the obtained results. In neither case, the in-vacuo dispersion effect was observed. The reason was a very miniature significance of

the in-vacuo dispersion in the energy range GRBAlpha operates in, subsequently making GRBAlpha unable to distinguish the minuscule microsecond effects with the temporal resolution in seconds. We propose one or a combination of the following effects causing the increasing and decreasing trend of the resulting curves:

- Spectral lags – a phenomenon appearing mostly in long gamma-ray bursts, causing the lower energy photons to leave the source of a gamma-ray burst later and therefore detect them in later times in comparison with the high energy photons. These lags have the potential to explain our 2 curves with decreasing features. The proposal is supported by the fact that for energy ranges in orders of GRBAlpha, the spectral lags are visible in orders of seconds, making them distinguishable with the GRBAlpha detector. We stress that the origin of spectral lag formation is uncertain and still under discussion.

- The most probable effect explaining the increasing trend of the second peak in GRB 221009A is the position of GRBAlpha during the detection. The satellite was situated on the North Pole and was approaching the outer Van Allen radiation belt. At these latitudes, the role of the background becomes significant, as well as the subsequent precession rotation with the wobble of the satellite. These effects could easily affect the appearance of the detected signal and outshine other, miniature effects.

We stress that, besides the observation of the in-vacuo dispersion, the goal of the data analysis was also to find secondary effects one needs to consider when studying the in-vacuo dispersion effect in the future. The main findings of this work were firstly the determination of the value of the fundamental scale for small satellites like GRBAlpha to detect the in-vacuo dispersion induced time delay — we found out that the needed scale must be in the orders of $10^{-7}\ E_{\mathrm{Pl}}$. Secondly, we tested that in the case of nano-satellites, there are other problems and factors the scientific community must deal with in order to study miniature and hardly detectable effects.

We concluded with a contribution to other possible explanations of the most energetic GRB 221009A detection besides the quantum gravity approach, such as sterile neutrinos, axion-like particles, and standard physical explanation. Finally, we presented a very promising future of quantum gravity phenomenology.

Bibliography

Abdo, A. A., Ackermann, M., Ajello, M., et al. 2009, Nature, 462, 331. https://doi.org/10.1038/nature08574

Abdo, A. A., Ackermann, M., Arimoto, M., et al. 2009, Science, 323, 1688. https://doi.org/10.1126/science.1169101

Ackermann, M., Asano, K., Atwood, W. B., et al. 2010, Astrophysical Journal, 716, 1178. https://iopscience.iop.org/article/10.1088/0004-637X/716/2/1178

Amelino-Camelia, G., Ellis, J., Mavromatos, N. E., et al. 1998, Nature, 393, 763. https://doi.org/10.1038/31647

Amelino-Camelia, G. 2002, Modern Physics Letters A, 17, 899. https://doi.org/10.1142/S0217732302007612

Amelino-Camelia, G. 2002, Physics Letters B, 528, 181. https://doi.org/10.1016/S0370-2693(02)01223-6

Amelino-Camelia, G. 2004, Thinking, Observing and Mining the Universe, 3. https://doi.org/10.1142/9789812702999_0001

Amelino-Camelia, G. & Smolin, L. 2009, Physical Review D, 80, 084017. https://doi.org/10.1103/PhysRevD.80.084017

Amelino-Camelia, G. 2013, Living Reviews in Relativity, 16, 5. https://doi.org/10.12942/lrr-2013-5

Amelino-Camelia, G., D'Amico, G., Rosati, G., et al. 2017, Nature Astronomy, 1, 0139. https://doi.org/10.1038/s41550-017-0139

Barthelmy, S. D., Barbier, L. M., Cummings, J. R., et al. 2005, Space Science Reviews, 120, 143. https://doi.org/10.1007/s11214-005-5096-3

Bedford, J. 2011, arXiv:1107.3967v3. https://arxiv.org/abs/1107.3967v3

Bodendorfer, N. 2016, arXiv:1607.05129v1. https://arxiv.org/abs/1607.05129v1

Bolmont, J. & Perennes, C. 2020, Journal of Physics Conference Series, 1586, 012033. https://doi.org/10.1088/1742-6596/1586/1/012033

Bolotin, Y. L., Tur, A. V., & Yanovsky, V. V. 2020, arXiv:2005.03984v1. https://arxiv.org/abs/2005.03984v1

Bolotin, Y. L. & Yanovsky, V. V. 2016, arXiv:1701.01022v1. https://arxiv.org/abs/1701.01022v1

Burderi, L., Di Salvo, T., Riggio, A., et al. 2020, Proceedings of the SPIE, 11444, 114444Y. https://doi.org/10.1117/12.2561779

Burderi, L., Sanna, A., Di Salvo, T., et al. 2021, Experimental Astronomy, 51, 1255. https://doi.org/10.1007/s10686-021-09745-5

Burns, E., Svinkin, D., Fenimore, E., et al. 2023, Astrophysical Journal, Letters, 946, L31. https://doi.org/10.3847/2041-8213/acc39c

Cao, Z., della Volpe, D., Liu, S., et al. 2019, arXiv:1905.02773v4. https://arxiv.org/abs/1905.02773v4

Casentini, C., Tavani, M., Pittori, C., et al. 2023, GRB Coordinates Network, Circular Service, No. 33412, 33412

Castro-Tirado, A. J., Sanchez-Ramirez, R., Hu, Y.-D., et al. 2022, GRB Coordinates Network, Circular Service, No. 32686, 32686

Chen, L., Lou, Y.-Q., Wu, M., et al. 2005, Astrophysical Journal, 619, 983. https://doi.org/10.1086/426774

Cheung, K. 2022, arXiv:2210.14178v2. https://arxiv.org/abs/2210.14178v2

Dafcikova, M., Ripa, J., Pal, A., et al. 2023, GRB Coordinates Network, Circular Service, No. 33418, 33418

Domínguez, A., Primack, J. R., Rosario, D. J., et al. 2011, Monthly Notices of the Royal Astronomical Society, 410, 2556. https://doi.org/10.1111/j.1365-2966.2010.17631.x

Doplicher, S., Fredenhagen, K., & Roberts, J. E. 1994, Physics Letters B, 331, 39. https://doi.org/10.1016/0370-2693(94)90940-7

Dzhappuev, D. D., Afashokov, Y. Z., Dzaparova, I. M., et al. 2022, The Astronomer's Telegram, 15669

Fermi GBM Team 2023, GRB Coordinates Network, Circular Service, No. 33405, 33405

Fiore, F., Burderi, L., Lavagna, M., et al. 2020, Proceedings of the SPIE, 11444, 114441R. https://doi.org/10.1117/12.2560680

Foley, S., McGlynn, S., Hanlon, L., et al. 2008, Astronomy and Astrophysics, 484, 143. https://doi.org/10.1051/0004-6361:20078399

Franceschini, A. & Rodighiero, G. 2017, Astronomy and Astrophysics, 603, A34. https://doi.org/10.1051/0004-6361/201629684

Frederiks, D., Svinkin, D., Lysenko, A. L., et al. 2023, arXiv:2302.13383v1. https://arxiv.org/abs/2302.13383v1

Gillanders, J., O'Connor, B., Dichiara, S., et al. 2023, GRB Coordinates Network, Circular Service, No. 33485, 33485

Guo, S.-Y., Khlopov, M., Wu, L., et al. 2023, arXiv:2301.03523v1. https://arxiv.org/abs/2301.03523v1

Hossenfelder, S. 2013, Living Reviews in Relativity, 16, 2. https://doi.org/10.12942/lrr-2013-2

Huang, Y., Hu, S., Chen, S., et al. 2022, GRB Coordinates Network, Circular Service, No. 32677, 32677

Koskinen, H. E. J. & Kilpua, E. K. J. 2022, Physics of Earth's Radiation Belts; Theory and Observations. ISBN: 978-3-030-82167-8. Cham: Springer International Publishing, 2022.

Kováčik, S. & Prešnajder, P. 2013, Journal of Mathematical Physics, 54, 102103. https://doi.org/10.1063/1.4826355

Kuulkers, E., Ferrigno, C., Kretschmar, P., et al. 2021, arXiv:2106.12446v1. https://arxiv.org/abs/2106.12446v1

Lacki, B. C. 2015, arXiv:1503.01509v1. https://arxiv.org/abs/1503.01509v1

Li, H. & Ma, B.-Q. 2021, Journal of High Energy Astrophysics, 32, 1. https://doi.org/10.1016/j.jheap.2021.07.001

Li, H. & Ma, B.-Q. 2023, Astroparticle Physics, 148, 102831. https://doi.org/10.1016/j.astropartphys.2023.102831

Li, H. & Ma, B.-Q. 2023, European Physical Journal C, 83, 192. https://doi.org/10.1140/epjc/s10052-023-11334-z

Massó, E. & Toldrà, R. 1995, Physical Review D, 52, 1755. https://doi.org/10.1103/PhysRevD.52.1755

Minkowski, H. 1909, Jahresbericht der Deutschen Mathematiker-Vereinigung, 18, 75

Navaneeth, P. K., Waratkar, G., Vibhute, A., et al. 2023, GRB Coordinates Network, Circular Service, No. 33415, 33415

Norris, J. P., Marani, G. F., & Bonnell, J. T. 2000, Astrophysical Journal, 534, 248. https://doi.org/10.1086/308725

Norris, J. P., Scargle, J. D., & Bonnell, J. T. 2001, Gamma-ray Bursts in the Afterglow Era, 40. https://doi.org/10.1007/10853853_9

Pál, A., Ohno, M., Mészáros, L., et al. 2020, Proceedings of the SPIE, 11444, 114444V. https://doi.org/10.1117/12.2561351

Pál, A., Ohno, M., Mészáros, L., et al. 2023, arXiv:2302.10048v2. https://arxiv.org/abs/2302.10048v2

Pillera, R., Bissaldi, E., Omodei, N., et al. 2022, The Astronomer's Telegram, 15656

Planck, M. 1900, Annalen der Physik, 306, 69. https://doi.org/10.1002/andp.19003060105

Ripa, J., Takahashi, H., Fukazawa, Y., et al. 2023, arXiv:2302.10047v2. https://arxiv.org/abs/2302.10047v2

Ronco, M., D'Amico, G., & Amelino-Camelia, G. 2022, Fifteenth Marcel Grossmann Meeting on General Relativity, 1529. https://doi.org/10.1142/9789811258251_0224

Thompson, D. J. & Wilson-Hodge, C. A. 2022, Handbook of X-ray and Gamma-ray Astrophysics. Edited by Cosimo Bambi and Andrea Santangelo, 29. https://doi.org/10.1007/978-981-16-4544-0_58-1

Vardanyan, V., Takhistov, V., Ata, M., et al. 2022, arXiv:2212.02436v1. https://arxiv.org/abs/2212.02436v1

Veres, P., Burns, E., Bissaldi, E., et al. 2022, GRB Coordinates Network, Circular Service, No. 32636, 32636

Wang, L. & Ma, B.-Q. 2023, arXiv:2304.01819v1. https://arxiv.org/abs/2304.01819v1

Xiong, S., Wang, C., Huang, Y., et al. 2023, GRB Coordinates Network, Circular Service, No. 33406, 33406

Zhao, Z.-C., Zhou, Y., & Wang, S. 2023, European Physical Journal C, 83, 92. https://doi.org/10.1140/epjc/s10052-023-11246-y

Zheng, Y. G., Kang, S. J., Zhu, K. R., et al. 2023, Physical Review D, 107, 083001. https://doi.org/10.1103/PhysRevD.107.083001

Zhu, J. & Ma, B.-Q. 2022, arXiv:2210.11376v2. https://arxiv.org/abs/2210.11376v2

Electronic sources

[e1] https://swift.gsfc.nasa.gov/about_swift/bat_desc.html (March 30, 2023)

[e2] https://www.grbnanosats.net/mediawiki/images/4/45/ (April 2, 2023)

[e3] http://side.iaa.es/EBL/ (May 7, 2023)

[e4] https://www.hermes-sp.eu/?p=10554 (May 13, 2023)

Appendix

Table 1.6: Selected GRBAlpha data sample of the first 30 seconds of GRB230307A.

chunk id	UTC time	longitude [°]	latitude [°]	altitude [km]
3716	2023-03-07 15:44:03.377768	100.230	-31.0215	550.885
3717	2023-03-07 15:44:04.377768	100.215	-31.0836	550.897
3718	2023-03-07 15:44:05.377768	100.200	-31.1458	550.909
3719	2023-03-07 15:44:06.377768	100.184	-31.2080	550.920
3720	2023-03-07 15:44:07.377768	100.169	-31.2702	550.932
3721	2023-03-07 15:44:08.377768	100.154	-31.3324	550.944
3722	2023-03-07 15:44:09.377768	100.138	-31.3946	550.955
3723	2023-03-07 15:44:10.377768	100.123	-31.4568	550.967
3724	2023-03-07 15:44:11.377768	100.108	-31.5189	550.979
3725	2023-03-07 15:44:12.377768	100.092	-31.5811	550.990
3726	2023-03-07 15:44:13.377768	100.077	-31.6433	551.002
3727	2023-03-07 15:44:14.377768	100.061	-31.7055	551.014
3728	2023-03-07 15:44:15.377768	100.046	-31.7676	551.025
3729	2023-03-07 15:44:16.377768	100.030	-31.8298	551.037
3730	2023-03-07 15:44:17.377768	100.015	-31.8920	551.049
3731	2023-03-07 15:44:18.377768	99.9993	-31.9542	551.060
3732	2023-03-07 15:44:19.377768	99.9837	-32.0163	551.072
3733	2023-03-07 15:44:20.377768	99.9682	-32.0785	551.084
3734	2023-03-07 15:44:21.377768	99.9526	-32.1407	551.096
3735	2023-03-07 15:44:22.377768	99.9370	-32.2028	551.107
3736	2023-03-07 15:44:23.377768	99.9214	-32.2650	551.119
3737	2023-03-07 15:44:24.377768	99.9058	-32.3271	551.131
3738	2023-03-07 15:44:25.377768	99.8902	-32.3893	551.143
3739	2023-03-07 15:44:26.377768	99.8746	-32.4514	551.154
3740	2023-03-07 15:44:27.377768	99.8589	-32.5136	551.166
3741	2023-03-07 15:44:28.377768	99.8432	-32.5758	551.178
3742	2023-03-07 15:44:29.377768	99.8276	-32.6379	551.190
3743	2023-03-07 15:44:30.377768	99.8119	-32.7001	551.202
3744	2023-03-07 15:44:31.377768	99.7961	-32.7622	551.213
3745	2023-03-07 15:44:32.377768	99.7804	-32.8243	551.225
3746	2023-03-07 15:44:33.377768	99.7646	-32.8865	551.237

Table 1.7: Selected GRBAlpha data sample of the first 30 seconds of GRB230307A. The last four columns present the four energy bands covering the whole energy range of the detector.

chunk id	Unix time [s]	channel 0	channel 1	channel 2	channel 3
3716	1678203843.377768	64	81	41	0
3717	1678203844.377768	73	88	37	0
3718	1678203845.377768	436	664	56	1
3719	1678203846.377768	834	1943	161	16
3720	1678203847.377768	1864	5008	531	97
3721	1678203848.377768	1439	3847	346	34
3722	1678203849.377768	1759	4769	443	86
3723	1678203850.377768	1915	4907	426	63
3724	1678203851.377768	2435	6273	631	139
3725	1678203852.377768	2242	5572	531	154
3726	1678203853.377768	1782	4112	382	57
3727	1678203854.377768	1823	4542	395	62
3728	1678203855.377768	1737	4054	354	52
3729	1678203856.377768	1551	3550	301	41
3730	1678203857.377768	1345	2857	234	26
3731	1678203858.377768	1483	3351	294	26
3732	1678203859.377768	1188	2475	203	16
3733	1678203860.377768	1177	2157	183	16
3734	1678203861.377768	950	1842	148	14
3735	1678203862.377768	763	1573	128	4
3736	1678203863.377768	443	763	77	0
3737	1678203864.377768	396	639	59	4
3738	1678203865.377768	901	1539	151	6
3739	1678203866.377768	771	1422	104	10
3740	1678203867.377768	827	1350	145	3
3741	1678203868.377768	654	1077	85	1
3742	1678203869.377768	647	915	109	2
3743	1678203870.377768	695	1046	89	3
3744	1678203871.377768	665	900	76	1
3745	1678203872.377768	471	570	71	1
3746	1678203873.377768	565	821	84	2